Journal of Materials Chemistry A

ROYAL SOCIETY OF CHEMISTRY

REVIEW

View Article Online
View Journal | View Issue

Check for updates

Cite this: J. Mater. Chem. A, 2022, 10, 5699

Support-based modulation strategies in single-atom catalysts for electrochemical CO_2 reduction: graphene and conjugated macrocyclic complexes

Zhanzhao Fu,[a] Mingliang Wu,[a] Yipeng Zhou,[a] Zhiyang Lyu,[b] Yixin Ouyang,[a] Qiang Li *[a] and Jinlan Wang *[a]

Received 21st October 2021
Accepted 24th November 2021

DOI: 10.1039/d1ta09069k

rsc.li/materials-a

The electrochemical CO_2 reduction reaction (CO_2RR) is a promising method to decrease the CO_2 concentration in the atmosphere and produce high value-added chemicals simultaneously. Catalysts play a central role in the CO_2RR system, and can determine the conversion efficiency and product species. Single-atom catalysts (SACs), a new class of catalysts, have been extensively employed in the CO_2RR due to their high activities, selectivity and maximum atom utilization efficiency. In this review, an overview of the recent progress of SACs for the CO_2RR is provided with respect to two types of catalyst supports including graphene (Gr)-based nanomaterials and conjugated macrocycle (CM)-based complexes. Specifically, we focus on significant influencing factors on the activity and selectivity of the modeled catalysts, such as heteroatom doping, ligand effects and bimetals. Insights on the intrinsic connection between electronic structures and catalytic properties are summarized. Moreover, the stability and the dynamic structural change of SACs under operating conditions are also discussed. Finally, some challenges and perspectives are raised for the future development of efficient SACs based on Gr and CM supports.

Published on 06 detsember 2021. Downloaded on 15.07.2024 7:26:52.

1. Introduction

The increasing concentration of CO_2 in the atmosphere has caused a series of environmental problems, including global warming and serious pollution issues.[1,2] According to statistics, the global average CO_2 concentration is higher than at any point in the past 800 000 years, which reached 405 ppm in 2017.[3,4] Thus, mitigating the atmospheric CO_2 concentration and utilizing it in an efficient way are urgent and important research challenges.[1] The electrochemical CO_2 reduction reaction (CO_2RR) powered by renewable electricity is a promising solution to address these challenges due to its high affordability.[5,6] However, a large driving force is needed to activate the linear CO_2 molecules, and the electrochemical CO_2RR is accompanied by complicated reaction mechanisms towards different products.[7] Hence, highly efficient and selective catalysts are essential to activate inert CO_2 molecules and to generate specific products with high selectivity.[8–10] Until now, various catalysts have been brought into the field for attaining high efficiency and selectivity, including heterogeneous solid catalysts, *e.g.*, metal/metal alloys, single-atom and non-metal catalysts, homogeneous molecular catalysts and their derivative heterogeneous molecular catalysts.[11–15]Among them, SACs have emerged as a new frontier in the catalysis field due to their various advantages over their bulk counterparts and other catalysts, including high atomic utilization efficiency (≈100%), high activity and high selectivity.[16–18]In this review, we will focus on two types of SACs in the CO_2RR, Gr-based SACs and CM-based SACs.[19,20]

For Gr-based SACs, they usually possess higher stability due to strong metal–substrate interactions.[21,22] So far, the active centers of most Gr-based SACs for the CO_2RR are metal atoms, which can be atomically dispersed on a modified Gr substrate. Among them, N-doped Gr-based SACs with different metal centers have been successfully prepared and exhibited excellent performance (*e.g.* high Faraday efficiency (~100%), high selectivity (above 90%), and high current density (hundreds of $mAcm^{-2}$)) in reducing CO_2 to different C1 products.[23–25] However, their activities need to be further improved to meet the requirement of industrial applications.[8] In contrast to Gr-based SACs, the structural information of CM-based SACs is available and well defined, which contributes to investigating the catalytic mechanism of the CO_2RR.[26] In addition, a well-defined active site structure can facilitate the establishment of the structure–mechanism–activity relationship. Furthermore, CM-based SACs are promising to achieve high activity and selectivity because ligands can be easily modulated by organic synthesis techniques to regulate the electronic structure of the active centers.[27] Although the catalytic performance of CM-based SACs can be improved by multiple methods, the biggest challenge limiting their practical applications is the low

[a]School of Physics, Southeast University, Nanjing, 211189, China. E-mail: qiang.li@seu.edu.cn; jlwang@seu.edu.cn

[b]School of Mechanical Engineering, Southeast University, Nanjing 211189, China

Published on 06 detsember 2021. Downloaded on 15.07.2024 7:26:52.

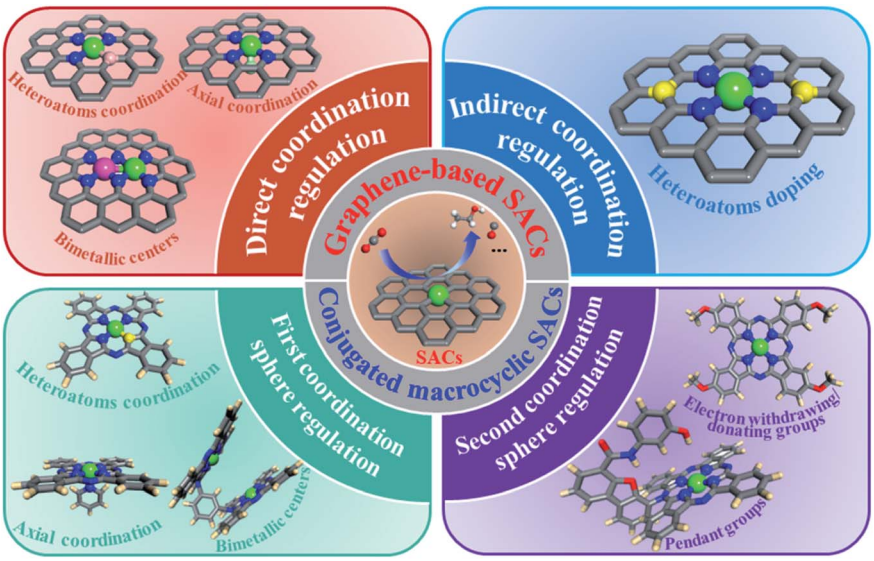

Fig. 1 Overview of two types of SACs for the CO_2RR and the corresponding strategies to regulate the catalytic activity.

stability.[28,29] Thus, conquering the stability problem faced by CM-based SACs is urgent to be addressed in the next stage.

In this review, as shown in Fig. 1, we aim to provide an overview of recent advances in the field of SACs for the CO_2RR, focusing on Gr and CM-based supports. For Gr-based SACs, various metal centers based on the Gr substrate are firstly described and the strategies that can improve their catalytic performance are then provided. Moreover, the state of the single atom during the reaction process is also discussed to determine the real active site of SACs. Theoretically, the structure–activity relationships for Gr-based SACs are clarified and provide some insights into bridging the relationship between theory and experiment. For CM-based SACs, strategies in tuning catalytic performances are systematically described from adjusting the first coordination sphere to the second coordination sphere. Next, effective methods to improve the stability of CM-based SACs are summarized to provide guidance for experimental researchers. Lastly, the relationship between Gr-based SACs and CM-based SACs is established, and some challenges and perspectives are raised to provide directions for the future development of SACs for the CO_2RR.

2. Fundamentals of the electrochemical CO_2RR

As a final product of fossil fuel combustion, CO_2 is thermodynamically very stable due to its non-polarity and strong C=O double bond, requiring large activation energy to drive its reduction to other products. The direct one-electron transfer to a linear CO_2 molecule to form bent CO_2^- requires a potential of −1.9 V *vs.* NHE (pH = 7, Table 1).[30] However, the standard reduction potentials of the CO_2RR to different products (Table 1, pH = 7) are usually much lower than that required to drive the first electron transfer.[31] Through the progression of multiple proton-coupled electron transfer processes, CO_2 can be reduced to various C1 products (*e.g.*, CO, HCOOH, CH_4, *etc.*) and C2 products (*e.g.*, C_2H_4, C_2H_6, C_2H_5OH, *etc.*). Given the singularity of single-atom active sites, almost no C2 products can be produced, and only C1 species are the main products produced by SACs.[32,33] As seen from Table 1, the standard reduction potentials of different C1 products are not too low but quite close to each other, suggesting the diversity of the C1 products. However, CO and HCOOH are the two main products and the deep reduction products including CH_3OH and CH_4 are barely reported. In addition, the competitive hydrogen evolution reaction (HER) is also a big challenge faced by the CO_2RR, which will greatly reduce the CO_2RR efficiency. Thus, it is extremely necessary to exploit catalysts with high selectivity, superior activity, and suitable stability to meet the practical applications of the CO_2RR.

Table 1 Standard reduction potentials of different products

Reduction products	Standard reduction potential *vs.* RHE, pH = 7
$CO_2+e^- \rightarrow CO_2^{\cdot -}$	$E^\circ = -1.49$V
$CO_2+2H^++2e^- \rightarrow CO + H_2O$	$E^\circ = -0.12$V
$CO_2+2H^++2e^- \rightarrow HCOOH$	$E^\circ = -0.20$V
$CO_2+4H^++4e^- \rightarrow HCHO + H_2O$	$E^\circ = -0.07$V
$CO_2+6H^++6e^- \rightarrow CH_3OH + H_2O$	$E^\circ = 0.03$V
$CO_2+8H^++8e^- \rightarrow CH_4+H_2O$	$E^\circ = 0.17$V
$2H^++2e^- \rightarrow H_2$	$E^\circ = -0.00$V

3. Gr-based SACs for CO_2 reduction

The single atom of SACs can be supported by various substrates, including graphene, carbon nanotubes, g-C_3N_4, graphyne, *etc.*34–37 Generally, these substrates possess high stability, superior conductivity and high abundance. Moreover, they can be modified by doping with different heteroatoms to provide

 This journal is © The Royal Society of Chemistry 2022

Published on 06 detsember 2021. Downloaded on 15.07.2024 7:26:52.

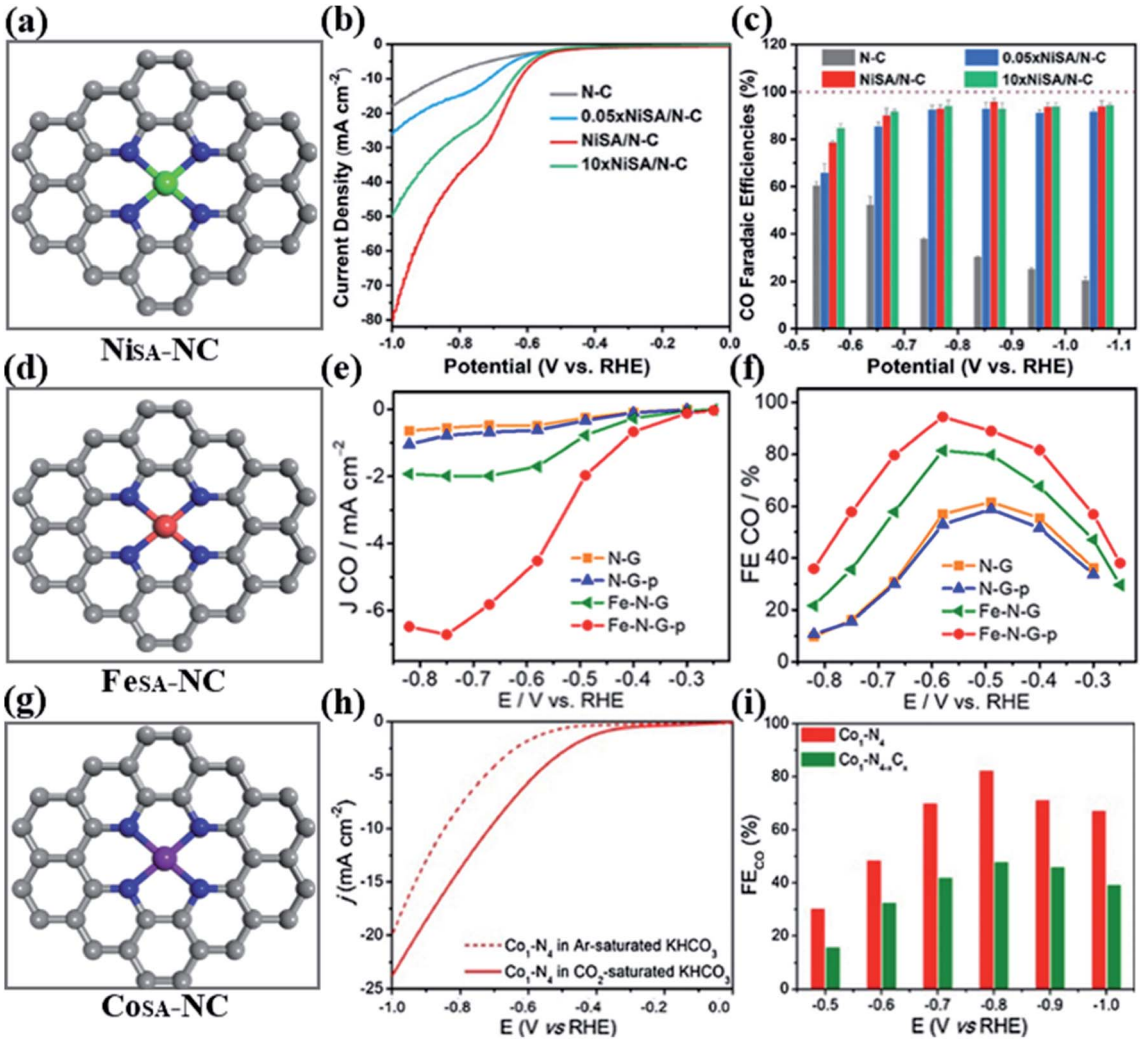

Fig. 2 (a) Structural model of Ni_{SA}-NC SACs. (b) Linear sweep voltammetry (LSV) curves at a scan rate of 10 mV s^{-1}. (c) FE_{CO} for N–C, 0.05xNi_{SA}/N–C, Ni_{SA}/N–C, and 10xNi_{SA}/N–C catalysts tested in CO_2-saturated 0.1 M $KHCO_3$ electrolytes. Reproduced with permission from ref. 53.Copyright 2020, Elsevier. (d) Structural model of Fe_{SA}-NC SACs. (e) CO partial current density. (f) FE_{CO} for N–G, N–G–p, Fe–N–G, and Fe–N–G–p. Reproduced with permission from ref. 55. Copyright 2020, American Chemical Society. (g) Structural model of Co_{SA}-NC SACs. (h) LSV curves of Co_1-N_4 were recorded in CO_2-saturated and Ar-saturated 0.1 M $KHCO_3$ (pH= 6.8) electrolytes. (i) FE_{CO} at selected potentials on Co_1-N_4 and Co_1-$N_{4-x}C_x$. Reproduced with permission from ref. 56.Copyright 2019, Elsevier.

a coordination environment to form strong metal–substrate interactions.[33] In this section, we will mainly focus on Gr-based SACs, due to their high conductivity, chemical robustness, porous structure, and adjustable composition.[38] And the discussions will extend from the changing of metal centers to regulating the catalytic activity by various strategies. Moreover, the real active sites of SACs and the real state of metal centers under operating conditions are also illustrated to provide deep insights on SACs.

3.1 Gr-based SACs with various metal centers

Due to the inertness of the intrinsic Gr surface, it is difficult for the pristine surface C atoms to coordinate with metal atoms directly, and the weak binding energy may result in the aggregation of single atoms.[39] Thus, it is necessary to introduce heteroatoms to provide the coordination environment for metal centers to form strong metal–substrate interactions. In general, N-doped Gr substrates are widely used to anchor single atoms,[40] and various SACs with the structure of MN_x ($x = 1$–4) have been successfully prepared by many synthesis methods,[41–43] including metal–organic framework (MOF) derived materials and conjugated macrocycle derived materials.[44,45] Moreover, advanced characterization techniques such as extended X-ray absorption fine structure (EXAFS), X-ray absorption near-edge structure (XANES), *etc.* have certified that most of these SACs possess the configuration of MN_4.[46–48]

The CO_2RR involves multi-electron transfer processes, and the activity of SACs can be determined by the binding strength between the reaction intermediates and the active sites. It is well known that metals with different distributions of d electrons can induce diverse interactions between reaction intermediates and active centers due to the different electron

Published on 06 detsember 2021. Downloaded on 15.07.2024 7:26:52.

Table 2 Summary of GR-based metal SACs for electrocatalytic CO_2 reduction

Catalysts	Main product	Potential (V *vs.* RHE)	Current density ($mAcm^{-2}$)	Faradaic efficiency (%)	Ref.
Mn-NC	CO	−0.55	−14.0	98.8	24
Fe-NC	CO	−0.58	−4.5	94	63
Fe-NC	CO	−0.8	−25	90	64
Fe-NC	CO	−0.64	−1.9	95	65
Fe-NC	CO	−0.46	−5.0	94	66
Fe-NC	CO	−0.76	−22.6	96	67
Co-NC	CO	−1.0	−15.8	82	56
Co-NC	CO	−0.73	−4.5	99.2	68
Co-NC	CO	−0.70	−14.9	98	69
Co-NC	CO	−0.60	−20	97	70
Ni-NC	CO	−0.85	−12	80	71
Ni-NC	CO	−0.79	−10	97	54
Ni-NC	CO	−0.70	−30	98	52
Ni-NC	CO	−1.0	−48.66	97	72
Ni-NC	CO	−0.68	−23	99	73
Cu-NC	CO	−0.7	−3.47	92	74
Cu-NC	CH_3OH	−0.9	NA	44	59
Cu-NC	CO	−0.9	∼−7.5	98	75
Cu-NC	CO	−0.74	−18.7	95.7	76
Cu-NC	CO	−1.0	−5	80.6	77
Zn-NC	CO	−0.43	−4.8	95	62
Zn-NC	CH_4	−1.15	−31.8	85	78
Zn-NC	CO	−0.44	−10.45	92.6	79
Zn-NC	CO	−0.44	−5	94	80
Cd-NC	CO	−0.728	−5.3	91.4	81
In-NC	HCOOH	−0.79	−6.8	80	48
In-NC	HCOOH	−0.65	−8.87	96	82
Sb-NC	HCOOH	−0.8	−2.5	94	83
Sn-NC	HCOOH	−0.95	−11.7	74.3	84

transfer abilities.[49–51]Among them, Ni-based N-doped graphene SACs are the most studied due to their high selectivity and Faraday efficiency (FE∼100%) for reduction of CO_2 to CO.[46,52] For example, as shown in Fig. 2a, Lu *et al.*[53] reported that Ni_{SA}/N–C possessed the highest CO_2RR activity (Fig. 2b), achieving 96% FE_{CO} with a current density of 26.4 $mAcm^{-2}$ at −0.86 V *vs.* RHE (Fig. 2c). The excellent CO_2RR activity of Ni SACs is attributed to the low binding energy toward *H and low-to-no binding of *CO, according to density functional theory (DFT) simulations. Yang *et al.* also demonstrated that Ni SACs displayed high intrinsic CO_2 reduction activity (FE = 97%) at a mild overpotential of 0.61 V in 0.5 M $KHCO_3$ solution.[47] The excellent CO_2RR activity of Ni SACs originated from the formation of a monovalent Ni(I) atomic center with a d^9 electronic configuration, which can spontaneously transfer an electron to the carbon 2p orbital in CO_2 to form the $CO_2^{\delta-}$ species to reduce the energy barrier for electrochemical CO_2 reduction. Some other studies have also certified that Ni SACs possess high CO_2RR activity to CO, which indicates that Ni SACs show great potential for practical applications.[41,54]

In addition to Ni-based SACs, Fe and Co-based SACs have also been reported for the CO_2RR, as shown in Fig. 2d–i.[55,56] When the CO_2RR was performed in a $KHCO_3$ electrolyte, Fe–N–C and Co–N–C SACs exhibited high CO_2RR efficiency (Fig. 2e and h); the maximum FE_{CO} can reach as high as 94% at −0.58 V *vs.* RHE on Fe–N–G–p SACs (Fig. 2f), and 82% FE can be achieved on Co_1-N_4 SACs (Fig. 2i). So far, Fe/Co/Ni N-doped Gr-based SACs are the most studied systems for the highly selective reduction of CO_2 to CO. Additionally, some other Gr-based SACs with different metal centers are also studied and summarized in Table 2. It can be noted that the main products of Mn, Fe, Co, Ni, and Cd-based SACs are CO, while the In, Sb, and Sn-based SACs mainly produce HCOOH. The diverse product selectivity of these metals can be ascribed to the different electron distributions, which can selectively stabilize key intermediates (*COOH *vs.* *OCHO) to produce CO or HCOOH.

Given the singularity of single-atom active sites, generally, only C1 products can be produced on SACs. In addition to CO and HCOOH, reports on deep reduction products (CH_4 and CH_3OH) are relatively rare, and the studied systems are mainly limited to Cu-SACs due to their favorable CO binding energies.[57,58] Yang *et al.* found that Cu-SACs reduced CO_2 to C1 products with about 100% FE at the potential of −0.9 V *vs.* RHE, and the FE of CH_3OH can reach 44% among all C1 products,[59] while Zheng *et al.* demonstrated that Cu-SACs can reduce CO_2 to CO with a maximum FE of 81% at a low potential of −0.50 V *vs.* RHE.[60]Apart from Cu SACs, Han *et al.* certified that Zn SACs can also reduce CO_2 to CH_4 with a maximum FE of 85% at a potential of −1.8 V *vs.* SCE.[61] Meanwhile, Yang *et al.* revealed that a FE_{CO} of 95% can be achieved on ZnN_4 SACs at a potential of −0.43 V *vs.* RHE.[62] It can be noticed that high potentials are needed to drive the further reduction of CO to produce deep reduction products (CH_3OH/CH_4).

 This journal is © The Royal Society of Chemistry 2022

Published on 06 detsember 2021. Downloaded on 15.07.2024 7:26:52.

3.2 Strategies to regulate the catalytic performance of Gr-SACs

There are various factors which can modulate the CO_2RR activity of SACs, such as electrical conductivity, electrochemically active surface area, surface morphology, *etc.*85 In this review, we will mainly focus on the intrinsic structure of the active sites based on several perspectives: (i) the structure–activity relationship can be well established; (ii) the precise structural regulation can bridge the theory and experiment; (iii) the intrinsic factor of changing the structure of the active centers can have more significant influence on the activity and selectivity of catalysts compared with external factors such as surface morphology and operating conditions.[86] In general, two strategies can be performed to engineer the coordination sphere of the active centers: (i) directly tuning the short-range coordination environment of the active sites; (ii) indirectly regulating the long-range interactions between heteroatoms and active centers on the substrates.

3.2.1 Direct coordination with metal centers. Atoms which directly coordinate with the metal center could have a significant impact on the electronic structure of the active sites.[87] Thus, directly changing the coordination atom at the metal center is the most intuitive way to tune the activity and selectivity of SACs. For example, Ni_{SA}-N_x-C catalysts with a controlled Ni–N coordination number from 4 to 2 were synthesized with Ni_{SA}-N_2-C exhibiting the best activity among all three Ni SACs, achieving the maximum FE_{CO} of 98% at −0.8 V *vs.* RHE (Fig. 3a–c).[88] Fu *et al.* also demonstrated that regulating the coordination environment of metal centers can not only enhance the catalytic activity but also generate deep reduction products.[89] As displayed in Fig. 3d, B, C, O, P and S were selected as doping atoms to tune the coordination environment of NiN_4 SACs, and it was found that CO was well captured after the introduction of B and

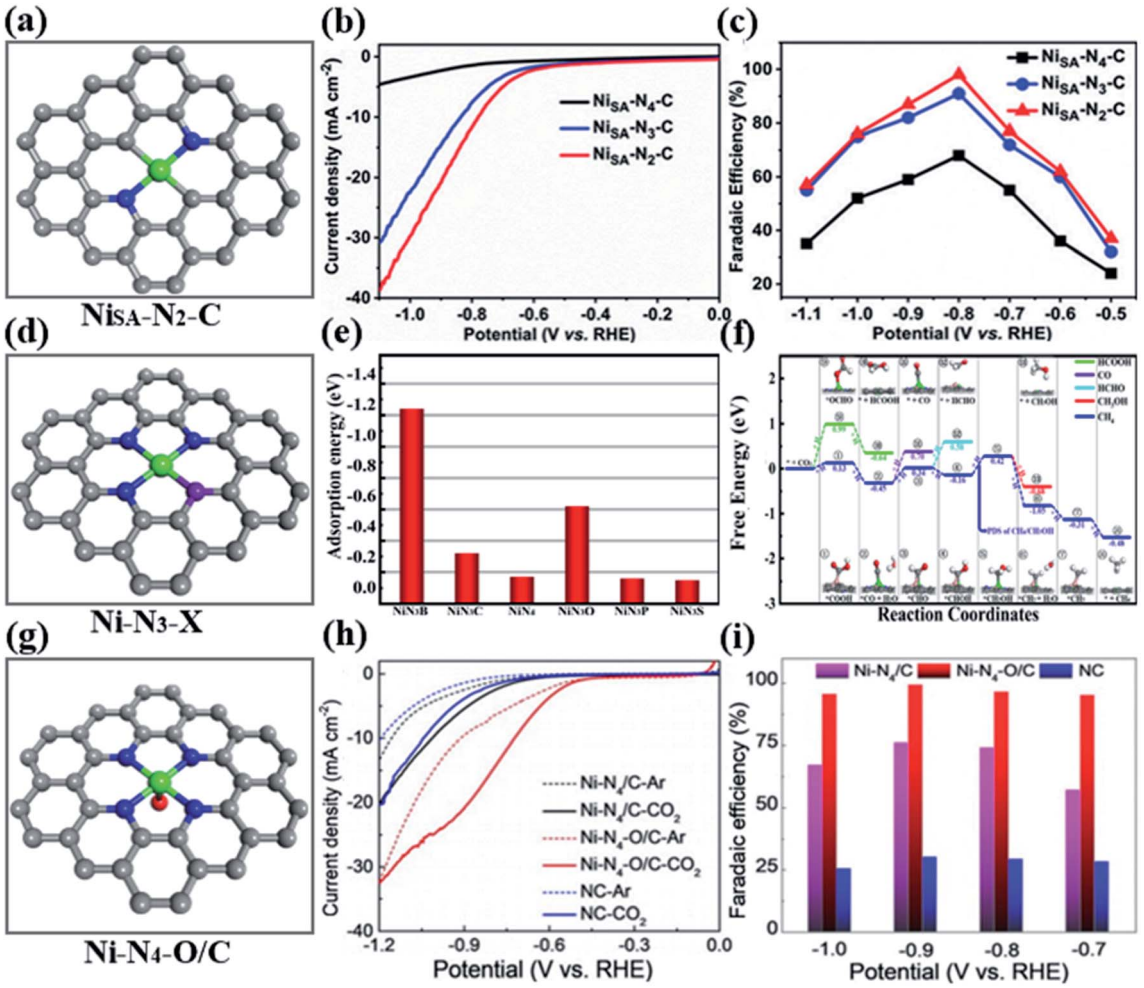

Fig. 3 (a) Structural model of Ni_{SA}-N_2-C. (b) LSV curves in the CO_2-saturated 0.5 M $KHCO_3$ electrolyte, and (c) FE_{CO} at different applied potentials over Ni_{SA}-N_x-C catalysts. Reprinted with permission from ref. 88.Copyright 2020, Wiley-VCH. (d) Doped structure of NiN_4. (e) CO adsorption energy of different doped structures in (d). (f) Free energy diagrams of the optimal CO_2RR pathway of CO, HCOOH, HCHO, CH_3OH and CH_4 catalyzed by NiN_3B, and insets are the coordination structures of the corresponding intermediates. Reprinted with permission from ref. 89.Copyright 2021, Royal Society of Chemistry. (g) Structural model of Ni-N_4-O/C. (h) Polarization curves of Ni-N_4-O/C (red), Ni-N_4/C (black), and NC (blue) in CO_2-saturated (solid) and Ar-saturated (dash) 0.5 M $KHCO_3$ solutions. (i) FE_{CO} at different potentials for Ni-N_4-O/C, Ni-N_4/C, and NC. Reprinted with permission from ref. 102.Copyright 2021, Wiley-VCH.

Published on 06 detsember 2021. Downloaded on 15.07.2024 7:26:52.

O atoms (Fig. 3e), which provides a prerequisite for the deep reduction of CO_2. By carefully considering the complete reaction pathway of the CO_2RR (Fig. 3f), B-doping (NiN_3B) stands out due to its high selectivity for CH_4 production with an ultralow onset-potential of −0.42 V. Moreover, the catalytic activity of NiN_3B can be further improved by tuning the B-doping concentration, with CH_4 catalyzed by NiN_2B_2-2 having an onset-potential as low as −0.20 V. The improved activity derives from the formation of Ni in the low charge state and the synergistic double active site between the Ni and B atoms. Table 3 summarizes recent studies on regulating the direct coordination atoms of the active centers to enhance the CO_2RR catalytic activity of SACs, including replacing N atoms with C/O/S atoms and reducing the coordination numbers of metal centers.

In addition to regulating the MN_4 fragment, the introduction of axial ligands into the metal center is another intuitive way to modulate the electronic structure of the active centers. For example, as exhibited in Fig. 3g, Wang *et al.* successfully introduced O atoms as an axial ligand into the Ni centers.[102] It was observed that Ni-N_4-O/C showed a higher catalytic activity for the CO_2R than its other counterparts (Fig. 3h), with a maximum FE_{CO} of 99.2% at −0.9 V *vs.* RHE (Fig. 3i). The calculated DOS illustrated that the electronic structure of the active Ni site was modified by the O atom, which significantly reduced the free energy barrier of the intermediates. Similarly, Zhang *et al.* successfully prepared (Cl, N)-Mn/G SACs with one axial chlorine atom, which displayed superior CO_2RR performance with a maximum FE_{CO} of 97% at −0.6 V *vs.* RHE.[103] The enhanced CO_2RR catalytic activity derives from the regulated electronic configuration induced by the ligand effect, which can promote the adsorption of CO_2/COOH* and the desorption of CO, and then lowers the barrier of the transition state.

According to the above discussions, we can conclude that directly regulating the coordination atoms (whether by replacing N atoms with other heteroatoms or introducing axial ligands) of the active center is the most intuitive and commonly used method to manipulate the activity of SACs, which can be ascribed to the direct regulation in the electronic structure of metal centers. However, in addition to C and O atoms, some other coordination heteroatoms (such as B, P, S, *etc.*) which are rarely studied can also be introduced to improve the CO_2RR activity of SACs, and more research studies should be conducted to enrich this field.

3.2.2 Indirect interaction with metal centers. Introducing heteroatoms which indirectly coordinate with metal centers can increase the available electron numbers and regulate the electronic structure of the active sites as well, and thus, it provides an alternative way to enhance the catalytic activity of SACs. For instance, Pan *et al.* reported that sulfur (S) incorporated Fe–N–C SACs with an Fe–S distance of around 4.50 Å exhibited the largest current density among their other counterparts (Fig. 4a and b).[25] DFT calculations revealed that S modification reduced the activation barrier of CO_2 on Fe-N_4, and thus significantly decreased the free energy changes for Fe-N_4+1S and Fe-N_4+2S (Fig. 4c). The improved CO_2 reduction performance of Fe–NS–C might be attributed to the increased available electron numbers of the Fe centers and the modified electronic configuration of the active sites. In addition to S atoms, F atoms have also been introduced into NiN_4 SACs, which exhibited enhanced CO_2RR activity compared to the NiN_4 counterpart.[104] DFT calculations elucidated that F-doping modulated the electronic configuration (increasing the charge density around Ni) of the central Ni-N_4 sites and thereby reduced the energy barrier for CO_2 activation, favorable to the generation of the key *COOH intermediate.

3.2.3 Metal–metal interactions. Compared with the aforementioned M-N_4 sites, incorporation with another metal center can also modulate the electronic structure of the active sites, which can induce electron transfer between two metals due to their different electronegativity. Moreover, the formed bimetallic centers can provide another site to stabilize reaction intermediates by bridging the adsorption configuration, thus bringing new opportunities for enhancing the catalytic performance.[105] Ouyang *et al.* found that the linear relationship can be

Table 3 Summary of metal SACs with different coordination environments for the CO_2RR

Catalysts	Main product	Potential (V *vs.* RHE)	Current density ($mAcm^{-2}$)	Faradaic efficiency (%)	Ref.
Mn-N_3	CO	−0.55	−14.0	98.8	24
Fe-N_5	CO	−0.46	−2.5	97	90
Ni-N_3-V	CO	−0.79	−11.0	97	54
Ni-N_2C_2	CO	−0.70	−18.5	98.7	91
Ni-N_2C_2	CO	−0.80	−10	98	88
Ni-N_3C_V	CO	−0.80	−6.64	95.6	92
Ni-N_3-V	CO	−0.90	−65.0	90	93
Ni-N_3S	CO	−0.80	−7.8	95	94
Ni-N_2-V_2	CO	−0.63	−30	97.8	95
Ni-C_3	CO	−0.74	−11	95	96
Ni-C_4	CO	−1.00	−35.0	96	97
Cu-N_2O_2	CH_4	−1.44	−40.0	78	98
Cu-N_2	CO	−0.50	−1.7	81	99
SnN_2O_2F	CO	−0.75	−8.5	95.2	100
BiN_3S	CO	−0.80	−10.24	98.3	101

 This journal is © The Royal Society of Chemistry 2022

Published on 06 detsember 2021. Downloaded on 15.07.2024 7:26:52.

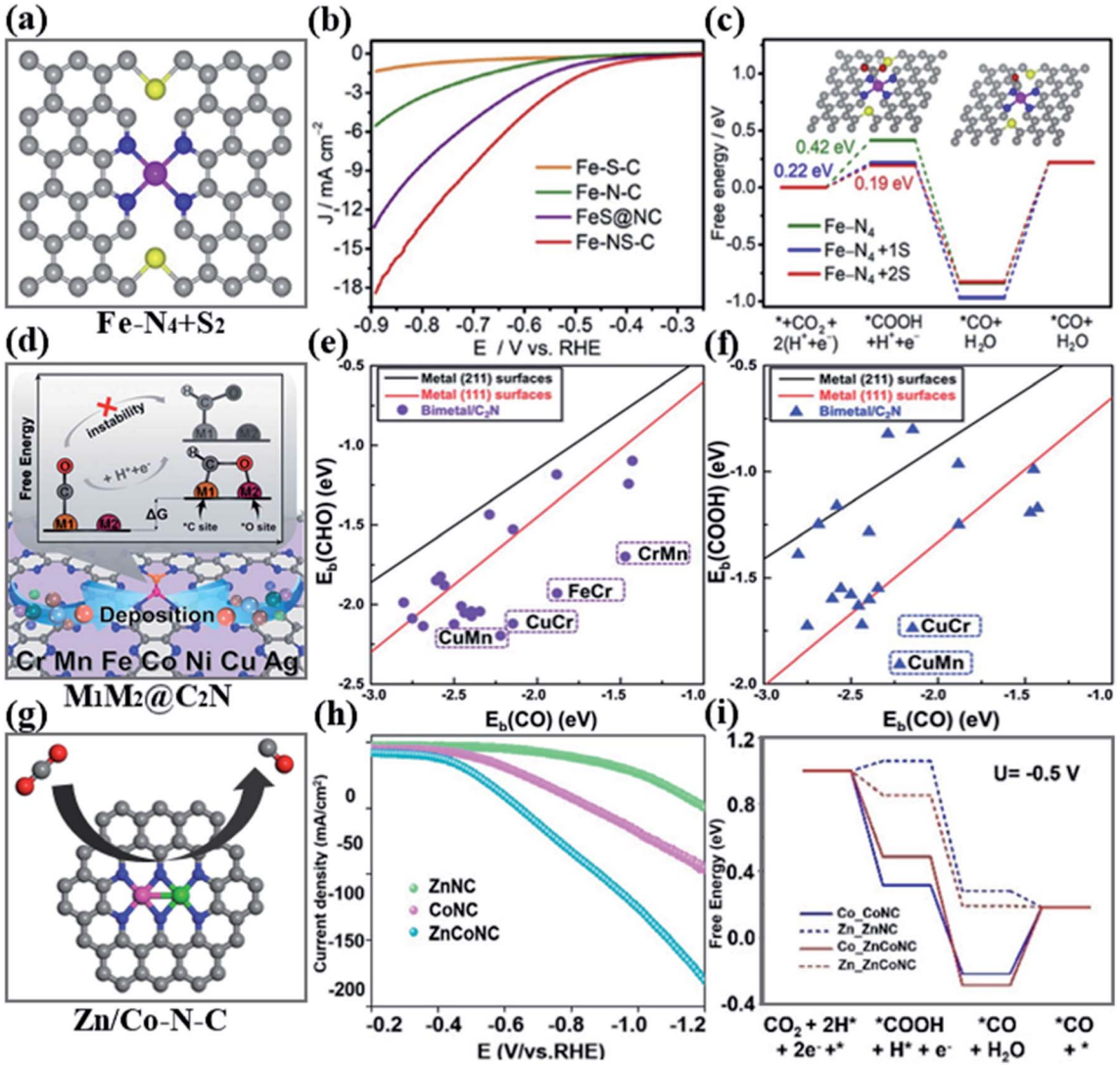

Fig. 4 (a) Atomic structure of proposed S-modified Fe-N_4 moieties. (b) CO_2RR polarization curves on Fe–S–C, Fe–N–C, FeS@NC, and Fe–NS–C. (c) Free energy diagrams of the CO_2RR at the electrode potential of $U = 0$ V. Insets are the optimized adsorption configurations of COOH* and CO* on Fe-N_4+2S. Reprinted with permission from ref. 25.Copyright 2020, Elsevier. (d) Design concept of monolayer C_2N supported heteronuclear transition-metal dimers to reduce the free energy change by stabilizing *CHO. (e) E_b(CHO) and E_b(CO), and (f) E_b(COOH) and E_b(CO) of the C_2N supported metal dimers and transition-metal surface. Reprinted with permission from ref. 106.Copyright 2020, Royal Society of Chemistry. (g) Illustration of the Zn/Co–N–C electrocatalytic CO_2RR to CO. (h) LSV curves of ZnNC, CoNC and ZnCoNC. (i) Calculated free energy for the pathway of CO_2 reduction to CO at −0.5 V on ZnNC, CoNC and ZnCoNC. Reprinted with permission from ref. 107.Copyright 2020, Wiley-VCH.

broken by forming bimetallic centers to achieve efficient CO_2RR *via* DFT calculations (Fig. 4d).[106] CuMn, CuCr, FeCr and MnCr supported by C_2N are located far from the conventional proportionality (Fig. 4e and f) and are promising candidates for reducing the CO_2RR overpotential and improving selectivity toward deep reduction products. Thus, utilizing the differences in carbophilicity and oxophilicity of metal atoms to form oxophilic and carbophilic bimetallic active sites can significantly enhance the catalytic activity of the CO_2RR by breaking the scaling relations. Zhu *et al.* employed a pyrolysis method to successfully synthesize a Zn/Co–N–C catalyst (Fig. 4g) which exhibited the lowest onset-potential of approximately −0.4 V and a much higher current density than Zn–N–C and Co–N–C (Fig. 4h).[107] Moreover, Zn/Co–N–C reached a FE_{CO} of 93.2% at −0.5 V, far exceeding those of other counterparts. DFT calculations revealed that the enhanced catalytic activity is ascribed to the advantage of CO_2 reduction to CO on Zn_Zn/CoNC, as there is downhill energy in both *COOH adsorption and *CO desorption (Fig. 4i). Moreover, CoNi and NiFe bimetallic catalysts have also been prepared and exhibited significantly enhanced CO_2RR activity.[108,109]

3.3 Real active sites of Gr-based SACs

Although Gr-based SACs have shown outstanding CO_2RR activity, there are still some controversies. For example, single atoms are often considered to be catalytic sites. However, the

Published on 06 detsember 2021. Downloaded on 15.07.2024 7:26:52.

calculated onset-potential at the single-atom site is very inconsistent with the experimental results, which inspired us to rethink the real active sites of SACs from the following two aspects: (i) whether the metal single atoms in SACs act as active sites or simply provide a facilitating role, or play both roles; (ii) whether M-N_4 is the real coordination configuration of metal centers, as the surface structure of Gr-based SACs involves multiple coordination configurations, including MN_3, MN_2 and even small clusters .

For the first aspect, Ni *et al.* recently reported that the intrinsic defects in the carbon plane of a single Fe-N_4 site are the active sites for the CO_2RR, and the defect-rich graphene-like porous carbon embedded with single-atom Fe-N_4 sites (DNG-SAFe) shows a tremendous priority to CO generation with a FE_{CO} of 90% at −0.75 and −0.85 V while that for NG-SAFe is less than 40% at the same potentials (Fig. 5a and b).[110] DFT calculations revealed that the free energy change of PDS on 585-Fe-N_4 is much lower than that on the pure 585 defect, Fe-N_4-N and Fe-N_4-NH, indicating a good synergistic effect between the 585 defect and Fe-N_4 moiety (Fig. 5c). These results indicated that the intrinsic defects in Fe–N–C SACs can be the real active sites in the CO_2RR.

For the second aspect, most studies indicate that a single Ni atom coordinated by four N atoms (NiN_4) is the active site for the reduction of CO_2 to CO, however, the calculation results based on the computational hydrogen electrode (CHE) model show a big gap between theoretical results and experimental results.[52,111,112] To resolve this problem, Zhao *et al.* evaluated the

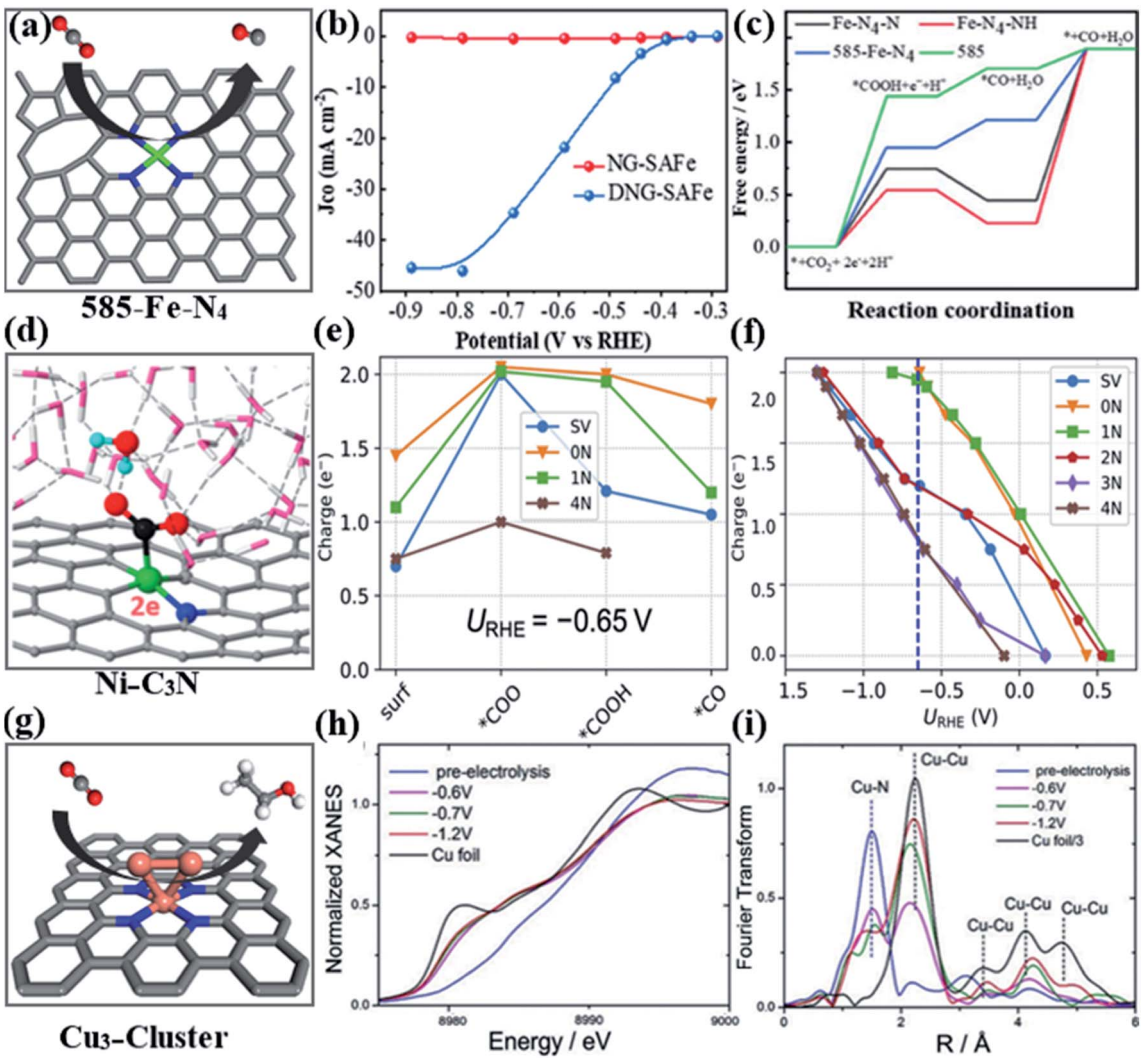

Fig. 5 (a) Illustration of the 585-Fe-N_4 electrocatalytic CO_2RR to CO. (b) J_{CO} of NG-SAFe and DNG-SAFe in 1 M $KHCO_3$ at different potentials. (c) Gibbs free energy diagrams (in eV) of the CO_2 RR over Fe-N_4-N and 585-Fe-N_4 sites. Reprinted with permission from ref. 110.Copyright 2021, Wiley-VCH. (d) Illustration of the $NiNC_3$ electrocatalytic CO_2RR in the explicit solvent model. (e) Charge capacity at $U_{RHE} = -0.65$ V for different sites with different adsorbates. (f) Charge capacity dependence on the potential for *COOH at different sites. Reprinted with permission from ref. 113.Copyright 2020, American Chemical Society. (g) Illustration of the Cu cluster formed *in situ* the electrocatalytic CO_2RR to CH_3CH_2OH. Operando XAS characterization of $Cu_{0.5}$NC at the Cu–K edge. (h) K-edge XANES spectra of $Cu_{0.5}$NC, (i) Fourier transform of the experimental EXAFS spectra of $Cu_{0.5}$NC under no potential applied (blue line), $Cu_{0.5}$NC during electrolysis at −0.6 V *vs.* RHE (pink line), at −0.7 V *vs.* RHE (green line), and at −1.2 V *vs.* RHE (red line) and metallic copper (black line). Reprinted with permission from ref. 114.Copyright 2019, Wiley-VCH.

 This journal is © The Royal Society of Chemistry 2022

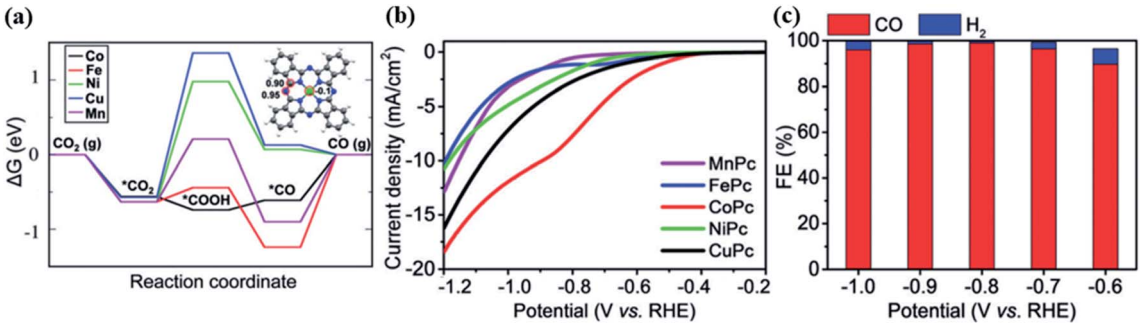

Fig. 6 Theoretical analysis of the electrocatalytic CO_2RR to CO by DFT calculations. (a) Calculated free-energy diagrams for all the MPc electrodes. The inset shows the adsorption energy of *COOH (in eV) on different sites of CoPc. (b) LSV tests in the CO_2-saturated electrolyte. (c) FE of CO and H_2 formation at different potentials for the CoPc sample. Reprinted with permission from ref. 130.Copyright 2018, Wiley-VCH.

Published on 06 detsember 2021. Downloaded on 15.07.2024 7:26:52.

reaction kinetic barriers of NiNC SACs by using *ab initio* molecular dynamics (AIMD) and a "slow-growth" sampling approach (Fig. 5d).[113] They found that the kinetic barriers on 0N and 1N sites were lower than those of other sites under a potential of −0.65 V *vs.* RHE for electrochemical steps due to the much higher charge capacity on the 0N, 1N, and SV sites (Fig. 6e). When non-electrochemical steps are considered, the CO desorption barrier for 1N was much lower than that of 0N (0.47 eV *vs.* 0.77 eV), demonstrating that the 1N site is more active. The calculated charge capacities of the 0N and 1N sites at $U_{RHE} = -0.65$ V were much higher than those of other sites, with *COOH as an example, which indicated that they should have lower electrochemical barriers and therefore be more active (Fig. 6f). In short, the 1N site ($NiNC_3$) has the highest activity and selectivity for the CO_2RR due to its higher charge capacity. The methods employed in this work can be extended to other systems to certify the real coordination environment of SACs, which will contribute to establishing the more precise structure–activity relationship.

3.4 Dynamic structural change of single atoms under operating conditions

Generally, the electrochemical CO_2RR is carried out in a reducing environment, which can result in the reduction of metal single atoms and lead to further aggregation into clusters. The reduction of coordinated metal single atoms is highly dependent on the intrinsic redox properties of metal centers. Recently, some studies have suggested that small agglomerates assembled from single atoms during the reduction reaction are the true active sites for the CO_2RR.[114,115] For example, Karapinar *et al.* found that the Cu oxidation state changed from +II to 0 when the applied potential was below −0.6 V *vs.* RHE, as revealed by the XANES spectra (Fig. 5h).[114] The Cu K-edge FT-EXAFS spectra of $Cu_{0.5}$NC recorded under operating conditions further demonstrated the appearance of Cu–Cu coordination, illustrating that metallic copper nanoparticles are extensively formed under electrocatalytic conditions (Fig. 5i). Thus, the high Faraday yield (FY) of the C_2-products on the Cu single site can be ascribed to the formed small Cu clusters during the reduction process (Fig. 5g). Xu *et al.* also observed that an immediate reduction from ionic to metallic Cu by *in situ* Cu k-edge XANES spectroscopy at −0.7 V and was mainly similar to the reduction of Cu^0 with a small Cu^+ (Cu_2O) component.[116] The EXAFS analysis further revealed that ultra-small Cu clusters with a coordination number of 2 (±0.9) or 3 (±1.2) can be formed during the CO_2RR. Therefore, in combination with the XANES and EXAFS results, the Cu_3 or Cu_4 clusters may serve as the real active sites for the reduction of CO_2 to ethanol. Thus, these studies have demonstrated that it is significantly important to study the real state of metal single atoms in the CO_2RR process, and can help us to track the real active sites of SACs in the catalytic process and contribute to us understanding the intrinsic reaction mechanism.

However, the specific dynamic structural evolution is discussed only on Cu–N–C SACs so far, which can be attributed to the following two aspects: (i) the bonding strength of Cu–N in the Cu–N–C catalyst is much weaker than that of other metal–N interactions, so that nitrogen coordination is not strong enough to stabilize the cationic Cu centers and leads to the aggregation of these atomically dispersed Cu atoms to form Cu clusters/nanoparticles;[117](ii) the products of the CO_2RR on other M–N–C SACs are usually CO/HCOOH, and thus little attention was paid to the "real" state of metal centers under the CO_2RR operating environment.[48,118] In addition to the CO_2RR, the dynamic changes of catalytic sites have also been observed in other catalytic systems. For example, Wang *et al.* found that the ceria supported gold clusters can form Au single atoms to act as the catalytic sites under CO oxidation operating conditions, and the Au single atoms can reintegrate back into the nanoparticle after the reaction.[119] Similarly, Moliner *et al.* found that Pt nanoparticles can reversibly transform into single atoms inside high-silica chabazite zeolite under different conditions.[120] These studies have demonstrated that the dynamic changes of single atoms generally occur under operating conditions, which should be more considered and studied in the future. Thus, the existence state of the metal atoms of other M–N–C SACs under a reducing environment should also be considered, and it is necessary to conduct *in situ* characterization on these systems to trace the real state of metal centers, which will contribute to establishing the accurate structure–activity relationship.

Published on 06 detsember 2021. Downloaded on 15.07.2024 7:26:52.

4. CM-based SACs for CO_2 reduction

Given the complexity of the surface structure of Gr-based SACs, it is difficult to ensure a uniform single-atom coordination structure (such as MN_4) on the surface, which may result in the coexistence of multiple coordination configurations (such as MN_3C, MN_2C_2, MNC_3, *etc.*). The unspecific coordination structure of Gr-based SACs is unfavorable to construct the structure–activity relationship. In contrast, CM-based SACs have crystalline patterns with well-defined structures, which allows for the construction of accurate structural models to analyze the multiple proton-coupled electron transfer processes involved in CO_2 reduction. This will help us to better understand the reduction mechanism and to establish the accurate structure–mechanism–activity relationship.[29] In general, CM-based SACs can be divided into homogeneous and heterogeneous forms.[8] In this review, heterogeneous CM-based SACs will be mainly discussed since they offer the advantages of long-term catalyst stability, promoted electron transfer, reduced catalyst usage, increased catalyst circulation and the like, as compared to homogeneous CM-based SACs.[121] So far, the most used heterogeneous CM-based SACs are species based on porphyrin (Pr) and phthalocyanine (Pc),[122,123] and a series of materials (such as MOFs, COFs and hybrid systems) including these species have been synthesized and exhibited favorable CO_2RR activity.[124–126]

4.1 CM-based SACs with different metal centers

With an explicit MN_4 structure, Pr and Pc-based SACs are expected to show a similar activity to Gr-based SACs (also characterized as MN_4 structures) with the same metals. As expected, such local structural similarity shows comparable activity and product selectivity, and the main product of Fe/Co/Ni based metals is CO for both Gr-based SACs and CM-based SACs.[15,53,56,122,127,128] However, some differences can also be found between these two types of systems. For instance, CoPc often shows high selectivity towards CO production in CM-based SACs, while the Ni-based metal is the preferred catalyst for Gr-based SACs.[111,129] As a typical example, a series of MPc (including M = Mn/Fe/Co/Ni/CuPc) were employed for the CO_2RR by Zhang *et al.*[130] DFT calculations were first performed to analyze the catalytic activity of different MPc, and there was a good linear relationship between E_{ad}(*CO) and E_{des}(*CO)/E_{for}(*COOH) with CoPc exhibiting the best catalytic performance for CO_2 electroreduction to CO (Fig. 6a). The LSV revealed that the CoPc catalyst exhibited the best catalytic activity (Fig. 6b) and showed the largest current density in a wide potential range with a maximum FE_{CO} as high as 99% at −0.8 V *vs.* RHE, much higher than that of other MPcs (Fig. 6c), demonstrating that CoPc possesses the best catalytic activity for the reduction of CO_2 to CO among MPcs.

4.2 Strategies to regulate the catalytic activity of CM-based SACs

4.2.1 Regulating the first coordination sphere. Similar to Gr-based SACs, introducing axial ligands and replacing the N atom of MN_4 centers with other heteroatoms have also been achieved on CM-based SACs. For instance, pyridine (Py) was introduced as an axial ligand to enhance the CO_2RR activity of CoPc (Fig. 7a).[131] A lowest onset-potential (Fig. 7b) with

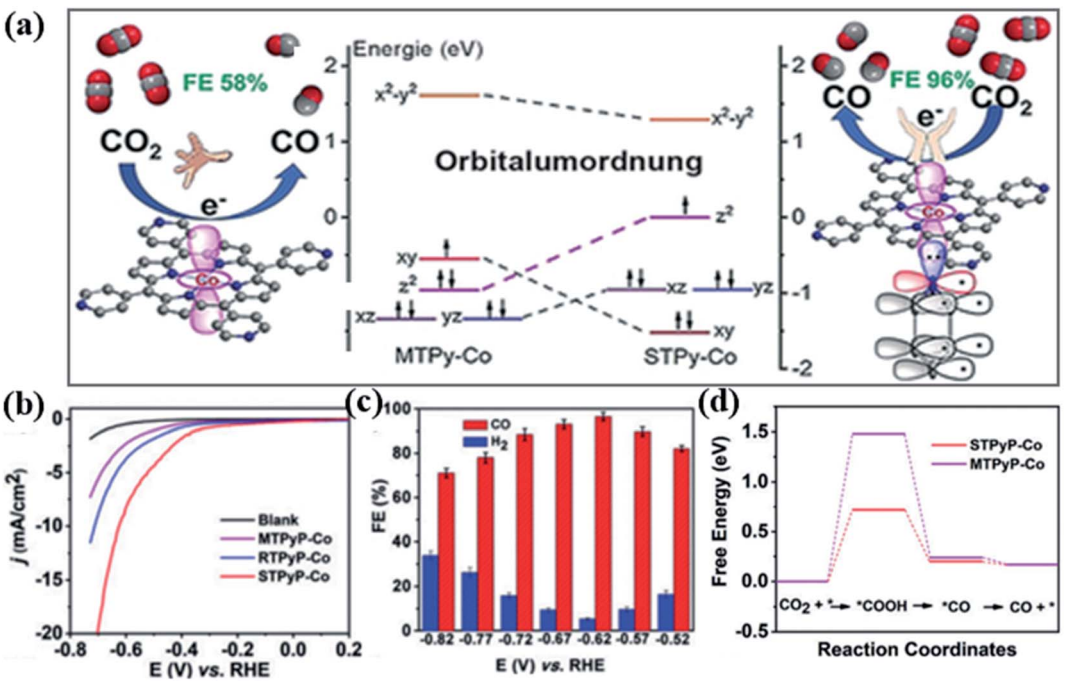

Fig. 7 (a) Schematic illustration of the intrinsic enhancement mechanism for the CO_2RR after introducing the axial Py ligand. (b) LSVs of MTPyP-Co, RTPyP-Co and STPyP-Co. (c) CO and H_2 FEs for STPyP-Co at different applied potentials. (d) Calculated free energy changes of CO_2 reduction to CO on STPyP-Co and MTPyP-Co. Reprinted with permission from ref. 131. Copyright 2019, Wiley-VCH.

 This journal is © The Royal Society of Chemistry 2022

Published on 06 detsember 2021. Downloaded on 15.07.2024 7:26:52.

a maximum FE_{CO} of 96 ± 1.8% at −0.62 V *vs.* RHE was achieved by ultrathin nanosheet tetra(4-pyridyl)porphyrin cobalt(II) (STPyP-Co) (Fig. 7c). The free energy change of the potential determining step on STPyP-Co was much lower than that of molecular tetra(4-pyridyl)porphyrin cobalt(II) (MTPyP-Co) as revealed by DFT calculations, demonstrating the positive effect of the Py ligands (Fig. 7d). Molecular orbital analysis showed that the Py ligands resulted in an increase in the energy level of the d_{z^2} orbital of the Co center making it more nucleophilic, which will enhance the CO_2 binding strength and facilitate the reduction of the free energy change during the CO_2RR (Fig. 7a). In addition to Py ligands, diphenyl sulfide has also been introduced into CoPr as the axial ligand to enhance the CO_2RR activity.[132]

Kim *et al.* reported that the CO_2RR activity of Ni-TPP can be significantly improved when replacing the N atom (NiN_4-TPP) with an O atom (NiN_3O-TPP), as shown in Fig. 8a.[133] By performing spectroscopic and computational studies, they revealed that the broken ligand-field symmetry is responsible for the enhanced CO_2RR activity, which will increase the redox potential of Ni to form Ni^I. Moreover, the stability of the Ni center can also be improved by this broken ligand-field symmetry induced redox effect. Therefore, replacing the N atom with other heteroatoms can break the intrinsic D_{4h} symmetry of the MN_4 centers, which will modulate the ligand-field distribution of the active sites and further regulate the redox potential of metal centers.

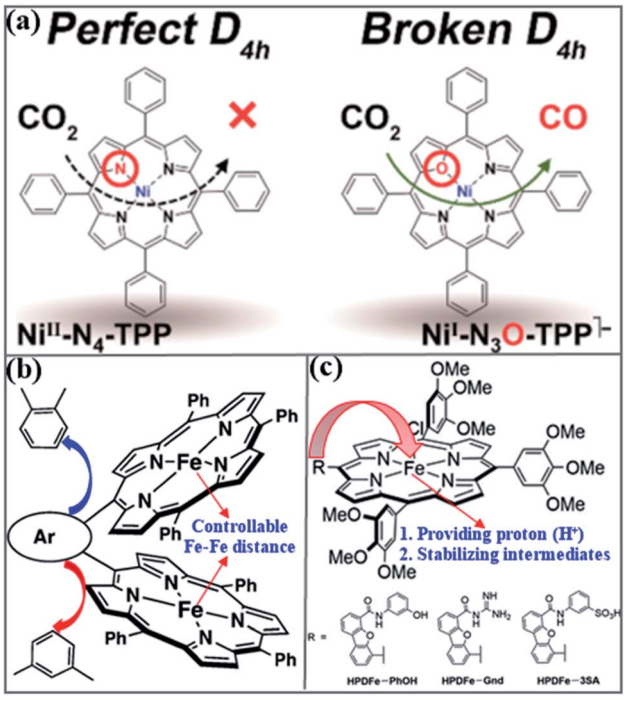

Fig. 8 (a) Concept principle of Ni-TPP complexes as CO_2RR catalysts and one N ligated atom was changed into the O atom. Reprinted with permission from ref. 133.Copyright 2021, American Chemical Society. (b) Chemical structures of the iron porphyrin dimers,*o*-Fe_2DTPP (above) and *m*-Fe_2DTPP (below). Reprinted with permission from ref. 134.Copyright 2015, Royal Society of Chemistry. (c) The structure of hangman Fe porphyrins and the corresponding substituent groups. Reprinted with permission from ref. 135.Copyright 2018, American Chemical Society.

Given the specific structure of the Pc/Pr conjugated macrocycle, it is unlikely to form a bimetallic center like that of Gr-based SACs. However, the concept of binuclear centers has also been applied to CM-based SACs to form two connected molecules *via* bridging ligands. The distance between the two metal centers can be manipulated by selecting a suitable bridging ligand, and the formed "pincer" structure can stabilize the reaction intermediates *via* a bridging geometry. As shown in Fig. 8b, a binuclear Fe porphyrin molecule $Fe_2$1 with an Fe–Fe distance of 3.4–4.0 Å was synthesized by Mohamed *et al.*[134] An electrochemical test illustrated that the catalytic current of $Fe_2$1 was six times higher than that of the Fe1 counterpart, which was derived from the proper separation of the two iron ions to provide a local push–pull mechanism with one Fe center acting as a Lewis base to push an electron pair to the CO_2 molecules and the second Fe center acting as a Lewis acid to promote C–O bond cleavage to form CO.

4.2.2 Stabilization of reaction intermediates by functional groups. Compared with Gr-based SACs, a prominent advantage of CM-based SACs is that ligands can be easily modified by organic synthesis techniques.[27] The introduced groups can provide H^+ or form a hydrogen bond with reaction intermediates, which will significantly enhance the H^+ transfer efficiency and stabilize the reaction intermediates. And the promotion effect depends on the intrinsic properties of the pendant groups (including pK_a value, relative positions and the numbers of the appended groups).[135–137] For example, Margarit *et al.* modified FeTPP with different pendant groups, and found that the pendant groups with different pK_a values can affect the CO_2RR performance of the Fe center to different degrees (Fig. 8c).[135] DFT calculations revealed that CO_2 can chemisorb on the Fe centers, and the H atoms of the pendant phenol (PhOH) and guanidinium (Gnd) groups can also interact with CO_2 by forming intramolecular H-bonds resulting in a decrease in free energy changes. However, these intramolecular H-bonds were not formed on the deprotonated benzenesulfonic acid (3SA), which further led to the electrostatic repulsion between the 3SA ions and TPP rings. Thus, the CO_2RR activity trend can be derived in the following sequence: FeTPP–PhOH > FeTPP–Gnd> FeTPP–3SA.

4.2.3 Promotion effect by electron withdrawing and donating groups. Inspired by the natural oxygen-evolving complex (OEC) of photosystem II, electron-withdrawing/donating groups can be introduced onto the second coordination sphere of CM-based SACs to enhance the CO_2RR activity.[138] The introduced electron-withdrawing/donating groups can engineer the redox potential of the active sites to regulate the redox-mediated CO_2RR mechanism. Cyano (CN) substituted CoPc had been successfully prepared and used for the CO_2RR (Fig. 9a).[139] The modified CoPc-CN exhibited higher catalytic activity, and the resulting hybrid catalyst exhibited >95% FE_{CO} in a wide potential range (Fig. 9b and c). Fluorine substituted CoPc had also been explored and showed high CO_2RR activity with a FE_{CO} >80% between −0.5 V and −0.9 V *vs.* RHE (Fig. 9d–

Published on 06 detsember 2021. Downloaded on 15.07.2024 7:26:52.

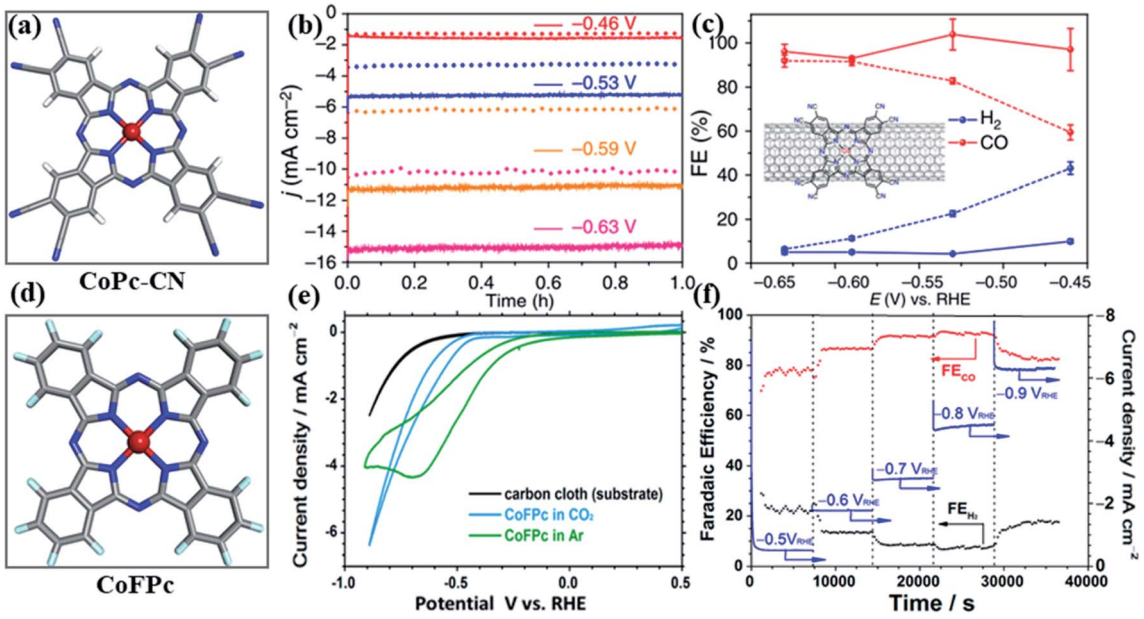

Fig. 9 (a) Structural model of CoPc-CN. (b) Chronoamperograms and (c) FEs of CO and H_2 at different potentials for the CoPc-CN/CNT (solid line) in comparison with those of the CoPc/CNT (dotted line). The inset in (b) shows the molecular structure of CoPc-CN anchored on the CNT. Reprinted with permission from ref. 139.Copyright 2017, Nature Publishing Group. (d) Structural model of CoFPc. (e) CVs of CoFPc on a carbon cloth electrode (1.0 cm^{-2}) under Ar (green trace) or CO_2 (blue trace). (f) Controlled potential electrolysis between −0.5 V and −0.9 V *vs.* RHE. Reprinted with permission from ref. 140.Copyright 2016, American Chemical Society.

f).[140] In addition to electron-withdrawing groups, an electron-donating methoxy-group had also been introduced onto Pc ligands to improve the catalytic activity of NiPc, and the enhanced catalytic activity was ascribed to the partial reduction of Ni centers following the introduction of electron-donating groups.[15]

4.3 Stability of heterogeneous CM-based SACs

Excellent stability of catalysts is one of the prerequisites for their practical applications. For CM-based SACs, generally, there are two stability issues. One is the separation of molecules from the substrates to aggregate into a molecular polymer blocking the active sites, and the other is the irreversible redox of metal centers or the Pr/Pc ligands under the CO_2RR operating conditions. Thus, appropriate strategies should be formulated to conquer these two stability issues, and some effective methods have been certified to significantly enhance the stability of CM-based SACs. Table 4 summarizes the stability performance of some typical CM-based SACs.

For the first stability issue faced by CM-based SACs, it can be seen that interactions between the catalysts and substrates play a critical role in the stability of the catalysts. For example, CoPc/OxC with non-covalent interactions undergo 30% current decay during the 6h electrochemical test. The other two examples (FePGF and FePGH-H) reported by Choi *et al.* showed low CO current density (<1 mA cm^{-2}) and it decreased with time.[141] For the covalently immobilized CM-based catalysts, CoPPCl/CNT-OH and CoPc-py-CNT showed high stability in the 12 h test with no significant decay in the current density and FE_{CO}.[142,143]

Table 4 Summary of the stability test results of benchmark CM-based SACs for the CO_2RR

Catalysts	Methods	Potential (V *vs.* RHE)	Time (h)	Current initial ($mAcm^{-2}$)	Current decay (%)	FE_{CO} initial (%)	FE decay (%)	Ref.
CoPc/CNT	Non-covalent	−0.63	10	−10.0	0	92	0	146
CoPc/OxC	Non-covalent	−0.73	6	−2.7	30	94	0	147
NiPc/CNT	Non-covalent	−0.68	0.7	−12.75	21.6	97	0	15
NiPc-OMe/CNT	Non-covalent	−0.61	40	−150	0	99.5	0	15
FePGF	Non-covalent	−0.59	24	−0.7	60	100	6	141
CoPPCl/CNT-OH	Covalent	−0.60	12	−25.0	4	98	3	142
CoPc-py-CNT	Covalent	−0.63	12	−0.41	15	90	3	143
Co-PMOF	Periodic	−0.80	36	−17.0 (2h)	0	100	6	144
D-P-CoPc	Periodic	−0.61	20	−2.4	0	94	—	148
CoPPc/CNT	Periodic	−0.54	24	−12	0	86	7	149

 This journal is © The Royal Society of Chemistry 2022

Published on 06 detsember 2021. Downloaded on 15.07.2024 7:26:52.

It is worth noting that CoPPCl/CNT-OH had the highest current density (25 mA cm^{-2}) in the table. In addition to covalent immobilization, the catalysts prepared by periodic immobilization also showed a stable current density and FE_{CO} during the stability tests. Among them, the Co-PMOF exhibited both high and stable current density for 36 h stability tests with only a 6% decay in FE_{CO}.[144] Thus, regulating the interactions between the catalysts and substrates to form covalent or periodic immobilization can be a favorable strategy to improve the stability of CM-based SACs.

For the other stability issue faced by CM-based SACs, Zhang *et al.* revealed that the XANES and the first derivative spectra of NiPc MDE under the CO_2RR environment showed a slight band edge shift to lower energies (~8346 eV), suggesting a partial reduction of the Ni center.[15] Moreover, they further demonstrated that the structural distortion occurred on the Ni-N_4 sites and may further decompose during the CO_2RR. The spectral shape and pre-edge peak can only be partially restored after the reaction, indicating that the degradation of Ni centers was irreversible. To control the redox of the catalysts, methoxy groups were introduced into the Pc ligands, and the stability of NiPc SACs can be significantly improved, showing stable performance at −150 mA cm^{-2} and >99.5% CO selectivity for 40 h in a gas diffusion electrode (GDE) device.[15] Similarly, Wu *et al.* introduced electron-abandoning substituents (–NH_2) on Pc ligands to improve the stability of CoPc SACs, and the enhanced stability was ascribed to the decreased reduction potential of CoPc induced by electron-donating substituents.[145]

5. Summary and perspectives

SACs with homogeneous atomically dispersed active metal centers exhibit excellent catalytic performance in energy conversion, especially the CO_2RR. With the well-defined structures, this type of material bridges experiment and theory to establish a structure–activity relationship and has become a hot topic recently in catalysis science and technology. This review summarizes SACs for the electro-reduction of CO_2, from Gr-based SACs to CM-based SACs, focusing on the factors that lead to a significant change of the activity and selectivity of catalysts. It is revealed that the catalytic activity is highly dependent on the discrete quantum states of the active centers and can be influenced by both the direct (or short-range) coordination environment and indirect (or long-range) interactions. Therefore, the electronic structure of SACs can be modulated to improve the activity and selectivity of the CO_2RR toward the target products. The stability of SACs and the dynamic structural change of the active sites under operating conditions are also manifested, which results in new mechanisms and products, thus changing the selectivity of SACs.

SACs endow the catalysts with multiple advantages, such as unique electronic structure, low-coordinated metal atoms, strong metal–support interactions, and maximum atom utilization. With the listed examples, it is revealed that CO_2 molecules can be converted into desired products by utilizing the moderate binding energy of different intermediates through corresponding reaction pathways, and the catalytic performance can be comparable to those of noble-metal benchmarks. After years of efforts from many experimental and theoretical groups, SACs have made great progress in many aspects, including large-scale synthesis, high-resolution characterization, high FE (~100%), even at industrial-scale current density (dozens of mAcm^{-2}) and favorable stability (hundreds of hours). However, the present activity and stability are still not sufficient for practical applications and many challenges remain to be addressed.

5.1 Active centers

Although both Gr- and CM-based SACs compose a structure of M-N_4, the differences can be clarified between them with the same metal centers applied based on recent studies. For example, the metal Co typically has the highest activity in CM-based SACs, while Ni is the most efficient metal to reduce CO_2 to CO in Gr-based SACs. In view of the structural similarity of their active centers, this gap is worth exploring to uncover the intrinsic structure–activity relationship. The difference can arise from many factors and the active center difference can be one of the main sources. In addition, it is reported that the real active site and the exact active configuration may not be the commonly accepted MN_4. Defective C sites, N sites, other coordination configurations like MN_1, and the synergistic effect with multiple sites can play an important role in the selectivity and activity of the catalysts.[150,151] For example, recent studies demonstrated that defects near the Fe-N_4 centers could be the real active sites of the CO_2RR.[110] This inspires us to consider whether this phenomenon is universal, especially for Ni-based SACs, due to the big gap between the theoretical and experimental results. In particular, N doped graphene has been illustrated to be highly efficient in reducing CO_2 to CO with a relatively low onset-potential, which further prompts us to rethink the role of Ni single-atom sites in the CO_2RR.[152,153] Therefore, sophisticated techniques and advanced analysis methods are highly desired to identify the structures and reaction pathways *in situ*. Together with systematic theoretical calculations and simulations, these results can validate the exact coordination configuration of the active centers and reveal the catalytic mechanism of SACs for the CO_2RR.

5.2 Promotion effect and deep reduction products

The direct change of the local environment of metal centers is proven to be the most effective way to tune the properties and catalytic performance of SACs, including heteroatom doping and introducing low coordination number and coordinated ligands. Such an effect is expected as the charge states of the metal center can be strongly modulated by short-range interactions. Meanwhile, the catalytic activity and stability of SACs, especially CM-based SACs, can also be enhanced by regulating long-range atoms and ligands. In nature, enzymes with various types of ligands are proven to be very efficient catalysts.[154] Therefore, the promotion mechanism by the long-range ligand effect should be revealed to improve the catalytic performance and design CO_2RR electrocatalysts more purposefully. Moreover, dual-metal sites, especially the heteronuclear type, which

Published on 06 detsember 2021. Downloaded on 15.07.2024 7:26:52.

are barely synthesized and reported, can also tune the electronic structure of the catalysts and obtain a better catalytic performance. Certainly, other factors can also play important roles in the catalytic performance of SACs, such as metal loading density, pH, electrolyte, and electrode contact.[155,156] Two-electron reduction products of CO and HCOOH are the major products from the CO_2RR on SACs. With many promotion strategies, deep reduction products (CH_4, CH_3OH, *etc.*) are more desirable due to their higher energy density.

5.3 Theoretical calculations

To simulate the electro-reduction process, most studies applied the CHE model to represent a very simple way from a thermochemical perspective, providing scaling relationships and descriptors such as binding energies and coordination numbers.[157,158] The CHE model can thus provide relatively credible trends based on DFT calculations, while the incorporation of the kinetic and reaction environment (solid–liquid interface) is further required to match the experiments quantitatively.[159] Therefore, it is necessary to include the solvation effect and applied potentials in the calculation models, and different approaches of either the explicit solvent or the implicit model have been proposed.[160,161] On one hand, the implicit approaches adopted by the polarizable continuum models based on the linear Poisson–Boltzmann equation can treat the interface with less computational effort.[162] However, the approximations cannot deal with strong interactions like hydrogen bonding and the local cation effect. On the other hand, AIMD takes the solvents, ions and cations explicitly, and records the changes of the interface and surroundings. The free energy profiles along defined specific reaction pathways can be collected statistically by enhanced sampling methods such as slow-growth, umbrella sampling, and metadynamics, and then the kinetics of the reaction can be obtained consequently.[163] Nevertheless, the limitation for AIMD is the expensive cost to sample over adequate trajectories to long time scales for reasonable analysis. In addition to the solvent effects and applied potentials, the commonly applied DFT methods with the generalized gradient approximation (GGA), PBE and PW91 functionals, for example, may result in inaccuracy for those systems with strong electron-correlations. For instance, reported adsorption energies of CO on SACs can be in a range from -0.6 to -1.2 eV; the large negative values suggest the possibility of further reduction of CO or the poisoning of SACs for desorption, which is contrary to experimental findings.[164] To overcome the deficiency, the DFT + U method can be a compromise solution and higher theoretical levels are needed, such as hybrid functionals, periodic MP2, and periodic coupled cluster methods, the latter two are very time-consuming and limited.

5.4 Dynamic structural change and stability

The survival of single-atom active sites under electrochemical reduction conditions is also worth exploring to uncover the intrinsic catalytic mechanism. Cu-based SACs provide a typical example of the dynamic structural change process during the CO_2RR, forming Cu clusters to produce C_{2+} products.[116] Therefore, *insitu* characterization is needed to monitor the structural evolution of SACs during the reaction, and time-resolved *in situ* measurements should be developed to reveal the real active sites. With the structural change of SACs during the reaction, the stability of the catalysts is a matter of concern. The deactivation mechanism of SACs has not been systematically studied so far, especially in theory. Therefore, continuous efforts should be made on this topic, both theoretically and experimentally. For the stability of CM-based SACs, although some progress has been made, it is still necessary to exploit new strategies to further enhance their stability to meet the needs of practical applications, for example, developing substrates which can form covalent interactions between the substrate and CM-based SACs by bridging ligands.

Although great progress has been made in recent years, many challenges and opportunities remain in developing SACs with high activity, selectivity and stability for the reduction of CO_2. As research and development continues, electrocatalytic reduction of CO_2 promises to alleviate future energy problems in a green and sustainable manner and to have a significant impact on the sustainability of our global energy economy.

Conflicts of interest

There are no conflicts of interest to declare.

Acknowledgements

This work was supported by the National Natural Science Foundation of China (Grant No. 22033002, 21525311, 21973011 and 22173018). The authors thank the computational resources from the Big Data Center of Southeast University and National Supercomputing Center of Tianjin.

References

1 S. Chu and A. Majumdar, *Nature*, 2012, **488**, 294–303.
2 M. Li, H. Wang, W. Luo, P. C. Sherrell, J. Chen and J. Yang, *Adv. Mater.*, 2020, **32**, e2001848.
3 B. Obama, *Science*, 2017, **355**, 126–129.
4 D. Luthi, M. Le Floch, B. Bereiter, T. Blunier, J. M. Barnola, U. Siegenthaler, D. Raynaud, J. Jouzel, H. Fischer, K. Kawamura and T. F. Stocker, *Nature*, 2008, **453**, 379–382.
5 Z. Yan, J. L. Hitt, J. A. Turner and T. E. Mallouk, *Proc. Natl. Acad. Sci. U. S. A.*, 2020, **117**, 12558–12563.
6 P. De Luna, C. Hahn, D. Higgins, S. A. Jaffer, T. F. Jaramillo and E. H. Sargent, *Science*, 2019, **364**, eaav3506.
7 R. Kortlever, J. Shen, K. J. Schouten, F. Calle-Vallejo and M. T. Koper, *J. Phys. Chem. Lett.*, 2015, **6**, 4073–4082.
8 F. Franco, C. Rettenmaier, H. S. Jeon and B. Roldan Cuenya, *Chem. Soc. Rev.*, 2020, **49**, 6884–6946.
9 J. Schneider, H. Jia, J. T. Muckerman and E. Fujita, *Chem. Soc. Rev.*, 2012, **41**, 2036–2051.
10 F. Li, A. Thevenon, A. Rosas-Hernandez, Z. Wang, Y. Li, C. M. Gabardo, A. Ozden, C. T. Dinh, J. Li, Y. Wang, J. P. Edwards, Y. Xu, C. McCallum, L. Tao, Z. Q. Liang,

 This journal is © The Royal Society of Chemistry 2022

Published on 06 detsember 2021. Downloaded on 15.07.2024 7:26:52.

M. Luo, X. Wang, H. Li, C. P. O'Brien, C. S. Tan, D. H. Nam, R. Quintero-Bermudez, T. T. Zhuang, Y. C. Li, Z. Han, R. D. Britt, D. Sinton, T. Agapie, J. C. Peters and E. H. Sargent, *Nature*, 2020, **577**, 509–513.
11 Y. Chen, S. Ji, C. Chen, Q. Peng, D. Wang and Y. Li, *Joule*, 2018, **2**, 1242–1264.
12 C. Kim, F. Dionigi, V. Beermann, X. Wang, T. Moller and P. Strasser, *Adv. Mater.*, 2019, **31**, e1805617.
13 D. M. Fernandes, A. F. Peixoto and C. Freire, *Dalton Trans.*, 2019, **48**, 13508–13528.
14 J. Collin and J. Sauvage, *Coord. Chem. Rev.*, 1989, **93**, 245–268.
15 X. Zhang, Y. Wang, M. Gu, M. Wang, Z. Zhang, W. Pan, Z. Jiang, H. Zheng, M. Lucero and H. Wang, *Nat. Energy*, 2020, **5**, 684–692.
16 B. Qiao, A. Wang, X. Yang, L. F. Allard, Z. Jiang, Y. Cui, J. Liu, J. Li and T. Zhang, *Nat. Chem.*, 2011, **3**, 634–641.
17 Y. Cheng, S. He, S. Lu, J. P. Veder, B. Johannessen, L. Thomsen, M. Saunders, T. Becker, R. De Marco, Q. Li, S. Z. Yang and S. P. Jiang, *Adv. Sci.*, 2019, **6**, 1802066.
18 X. Zhao and Y.-G. Li, *Rare Met.*, 2020, **39**, 455–457.
19 C. S. Diercks, Y. Liu, K. E. Cordova and O. M. Yaghi, *Nat. Mater.*, 2018, **17**, 301–307.
20 L. Wang, W. Chen, D. Zhang, Y. Du, R. Amal, S. Qiao, J. Wu and Z. Yin, *Chem. Soc. Rev.*, 2019, **48**, 5310–5349.
21 A. Wang, J. Li and T. Zhang, *Nat. Rev. Chem.*, 2018, **2**, 65–81.
22 S. Ji, Y. Chen, X. Wang, Z. Zhang, D. Wang and Y. Li, *Chem. Rev.*, 2020, **120**, 11900–11955.
23 Q. Fan, P. Hou, C. Choi, T. S. Wu, S. Hong, F. Li, Y. L. Soo, P. Kang, Y. Jung and Z. Sun, *Adv. Energy Mater.*, 2020, **10**, 1903068.
24 J. Feng, H. Gao, L. Zheng, Z. Chen, S. Zeng, C. Jiang, H. Dong, L. Liu, S. Zhang and X. Zhang, *Nat. Commun.*, 2020, **11**, 4341.
25 F. Pan, B. Li, E. Sarnello, S. Hwang, Y. Gang, X. Feng, X. Xiang, N. M. Adli, T. Li, D. Su, G. Wu, G. Wang and Y. Li, *Nano Energy*, 2020, **68**, 104384.
26 J. Wang, S. Dou and X. Wang, *Sci. Adv.*, 2021, **7**, eabf3989.
27 F. A. A. Paz, J. Klinowski, S. M. Vilela, J. P. Tome, J. A. Cavaleiro and J. Rocha, *Chem. Soc. Rev.*, 2012, **41**, 1088–1110.
28 D. Yang, B. Ni and X. Wang, *Adv. Energy Mater.*, 2020, **10**, 2001142.
29 E. Boutin, L. Merakeb, B. Ma, B. Boudy, M. Wang, J. Bonin, E. Anxolabéhère-Mallart and M. Robert, *Chem. Soc. Rev.*, 2020, **49**, 5772–5809.
30 J.-M. Savéant, *Chem. Rev.*, 2008, **108**, 2111–2112.
31 A. J. Gottle and M. T. M. Koper, *Chem. Sci.*, 2017, **8**, 458–465.
32 M. Li, H. Wang, W. Luo, P. C. Sherrell, J. Chen and J. Yang, *Adv. Mater.*, 2020, **32**, 2001848.
33 T. N. Nguyen, M. Salehi, Q. V. Le, A. Seifitokaldani and C. T. Dinh, *ACS Catal.*, 2020, **10**, 10068–10095.
34 W. Xiong, H. Li, H. Wang, J. Yi, H. You, S. Zhang, Y. Hou, M. Cao, T. Zhang and R. Cao, *Small*, 2020, **16**, e2003943.
35 S. Zhao, Y. Cheng, J.-P. Veder, B. Johannessen, M. Saunders, L. Zhang, C. Liu, M. F. Chisholm, R. De Marco and J. Liu, *ACS Appl. Energy Mater.*, 2018, **1**, 5286–5297.
36 P. Chen, B. Lei, X. a. Dong, H. Wang, J. Sheng, W. Cui, J. Li, Y. Sun, Z. Wang and F. Dong, *ACS Nano*, 2020, **14**, 15841–15852.
37 Y. Ni, L. Miao, J. Wang, J. Liu, M. Yuan and J. Chen, *Phys. Chem. Chem. Phys.*, 2020, **22**, 1181–1186.
38 X. Zhu, C. Hu, R. Amal, L. Dai and X. Lu, *Energy Environ. Sci.*, 2020, **13**, 4536–4563.
39 P. Wang, D. Zhao and L. Yin, *Energy Environ. Sci.*, 2021, **14**, 1794–1834.
40 W. Ju, A. Bagger, G.-P. Hao, A. S. Varela, I. Sinev, V. Bon, B. R. Cuenya, S. Kaskel, J. Rossmeisl and P. Strasser, *Nat. Commun.*, 2017, **8**, 1–9.
41 Q. Fan, P. Hou, C. Choi, T. S. Wu, S. Hong, F. Li, Y. L. Soo, P. Kang, Y. Jung and Z. Sun, *Adv. Energy Mater.*, 2019, **10**, 1903068.
42 L. Jiao, W. Yang, G. Wan, R. Zhang, X. Zheng, H. Zhou, S. H. Yu and H. L. Jiang, *Angew. Chem.*, 2020, **132**, 20770–20776.
43 W. Bi, X. Li, R. You, M. Chen, R. Yuan, W. Huang, X. Wu, W. Chu, C. Wu and Y. Xie, *Adv. Mater.*, 2018, **30**, e1706617.
44 Z. Song, L. Zhang, K. Doyle-Davis, X. Fu, J. L. Luo and X. Sun, *Adv. Energy Mater.*, 2020, **10**, 2001561.
45 Y. Wang, Z. Jiang, X. Zhang, Z. Niu, Q. Zhou, X. Wang, H. Li, Z. Lin, H. Zheng and Y. Liang, *ACS Appl. Mater. Interfaces*, 2020, **12**, 33795–33802.
46 D. M. Koshy, S. Chen, D. U. Lee, M. B. Stevens, A. M. Abdellah, S. M. Dull, G. Chen, D. Nordlund, A. Gallo and C. Hahn, *Angew. Chem.*, 2020, **132**, 4072–4079.
47 H. B. Yang, S.-F. Hung, S. Liu, K. Yuan, S. Miao, L. Zhang, X. Huang, H.-Y. Wang, W. Cai and R. Chen, *Nat. Energy*, 2018, **3**, 140–147.
48 P. Lu, X. Tan, H. Zhao, Q. Xiang, K. Liu, X. Zhao, X. Yin, X. Li, X. Hai and S. Xi, *ACS Nano*, 2021, **15**, 5671–5678.
49 S. Back, J. Lim, N.-Y. Kim, Y.-H. Kim and Y. Jung, *Chem. Sci.*, 2017, **8**, 1090–1096.
50 J.-H. Liu, L.-M. Yang and E. Ganz, *J. Mater.Chem. A*, 2019, **7**, 3805–3814.
51 L. Gong, D. Zhang, C. Y. Lin, Y. Zhu, Y. Shen, J. Zhang, X. Han, L. Zhang and Z. Xia, *Adv. Energy Mater.*, 2019, **9**, 1902625.
52 W. Ren, X. Tan, X. Chen, G. Zhang, K. Zhao, W. Yang, C. Jia, Y. Zhao, S. C. Smith and C. Zhao, *ACS Catal.*, 2020, **10**, 13171–13178.
53 Y. Lu, H. Wang, P. Yu, Y. Yuan, R. Shahbazian-Yassar, Y. Sheng, S. Wu, W. Tu, G. Liu and M. Kraft, *Nano Energy*, 2020, **77**, 105158.
54 Y. J. Sa, H. Jung, D. Shin, H. Y. Jeong, S. Ringe, H. Kim, Y. J. Hwang and S. H. Joo, *ACS Catal.*, 2020, **10**, 10920–10931.
55 F. Pan, B. Li, E. Sarnello, Y. Fei, X. Feng, Y. Gang, X. Xiang, L. Fang, T. Li and Y. H. Hu, *ACS Catal.*, 2020, **10**, 10803–10811.
56 Z. Geng, Y. Cao, W. Chen, X. Kong, Y. Liu, T. Yao and Y. Lin, *Appl. Catal., B*, 2019, **240**, 234–240.
57 Y. Cai, J. Fu, Y. Zhou, Y.-C. Chang, Q. Min, J.-J. Zhu, Y. Lin and W. Zhu, *Nat. Commun.*, 2021, **12**, 1–9.

Published on 06 detsember 2021. Downloaded on 15.07.2024 7:26:52.

58 H. Bao, Y. Qiu, X. Peng, J.-a. Wang, Y. Mi, S. Zhao, X. Liu, Y. Liu, R. Cao and L. Zhuo, *Nat. Commun.*, 2021, **12**, 1–9.
59 H. Yang, Y. Wu, G. Li, Q. Lin, Q. Hu, Q. Zhang, J. Liu and C. He, *J. Am. Chem. Soc.*, 2019, **141**, 12717–12723.
60 W. Zheng, J. Yang, H. Chen, Y. Hou, Q. Wang, M. Gu, F. He, Y. Xia, Z. Xia and Z. Li, *Adv. Funct.Mater.*, 2020, **30**, 1907658.
61 L. Han, S. Song, M. Liu, S. Yao, Z. Liang, H. Cheng, Z. Ren, W. Liu, R. Lin and G. Qi, *J. Am. Chem. Soc.*, 2020, **142**, 12563–12567.
62 F. Yang, P. Song, X. Liu, B. Mei, W. Xing, Z. Jiang, L. Gu and W. Xu, *Angew. Chem., Int. Ed.*, 2018, **57**, 12303–12307.
63 F. Pan, B. Li, E. Sarnello, Y. Fei, X. Feng, Y. Gang, X. Xiang, L. Fang, T. Li, Y. H. Hu, G. Wang and Y. Li, *ACS Catal.*, 2020, **10**, 10803–10811.
64 N. Mohd Adli, W. Shan, S. Hwang, W. Samarakoon, S. Karakalos, Y. Li, D. A. Cullen, D. Su, Z. Feng and G. Wang, *Angew. Chem.*, 2021, **133**, 1035–1045.
65 S. Wu, X. Lv, D. Ping, G. Zhang, S. Wang, H. Wang, X. Yang, D. Guo and S. Fang, *Electrochim. Acta*, 2020, **340**, 135930.
66 Y. Wang, M. Wang, Z. Zhang, Q. Wang, Z. Jiang, M. Lucero, X. Zhang, X. Li, M. Gu and Z. Feng, *ACS Catal.*, 2019, **9**, 6252–6261.
67 F. Pan, B. Li, E. Sarnello, Y. Fei, Y. Gang, X. Xiang, Z. Du, P. Zhang, G. Wang and H. T. Nguyen, *ACS Nano*, 2020, **14**, 5506–5516.
68 Y. Pan, R. Lin, Y. Chen, S. Liu, W. Zhu, X. Cao, W. Chen, K. Wu, W.-C. Cheong and Y. Wang, *J. Am. Chem. Soc.*, 2018, **140**, 4218–4221.
69 P. Hou, W. Song, X. Wang, Z. Hu and P. Kang, *Small*, 2020, **16**, 2001896.
70 H. Yang, Q. Lin, Y. Wu, G. Li, Q. Hu, X. Chai, X. Ren, Q. Zhang, J. Liu and C. He, *Nano Energy*, 2020, **70**, 104454.
71 T. Möller, W. Ju, A. Bagger, X. Wang, F. Luo, T. Ngo Thanh, A. S. Varela, J. Rossmeisl and P. Strasser, *Energy Environ. Sci.*, 2019, **12**, 640–647.
72 C. Zhao, Y. Wang, Z. Li, W. Chen, Q. Xu, D. He, D. Xi, Q. Zhang, T. Yuan, Y. Qu, J. Yang, F. Zhou, Z. Yang, X. Wang, J. Wang, J. Luo, Y. Li, H. Duan, Y. Wu and Y. Li, *Joule*, 2019, **3**, 584–594.
73 T. Zheng, K. Jiang, N. Ta, Y. Hu, J. Zeng, J. Liu and H. Wang, *Joule*, 2019, **3**, 265–278.
74 F. Yang, X. Mao, M. Ma, C. Jiang, P. Zhang, J. Wang, Q. Deng, Z. Zeng and S. Deng, *Carbon*, 2020, **168**, 528–535.
75 H. Cheng, X. Wu, X. Li, X. Nie, S. Fan, M. Feng, Z. Fan, M. Tan, Y. Chen and G. He, *Chem. Eng. J.*, 2021, **407**, 126842.
76 J. Feng, L. Zheng, C. Jiang, Z. Chen, L. Liu, S. Zeng, L. Bai, S. Zhang and X. Zhang, *Green Chem.*, 2021, **23**, 5461–5466.
77 C. Xu, X. Zhi, A. Vasileff, D. Wang, B. Jin, Y. Jiao, Y. Zheng and S.-Z. Qiao, *Small Struct.*, 2020, **2**, 2000058.
78 L. Han, S. Song, M. Liu, S. Yao, Z. Liang, H. Cheng, Z. Ren, W. Liu, R. Lin, G. Qi, X. Liu, Q. Wu, J. Luo and H. L. Xin, *J. Am. Chem. Soc.*, 2020, **142**, 12563–12567.
79 M. Fang, X. Wang, X. Li, Y. Zhu, G. Xiao, J. Feng, X. Jiang, K. Lv, Y. Zhu and W. F. Lin, *ChemCatChem*, 2021, **13**, 603–609.
80 N. Wang, Z. Liu, J. Ma, J. Liu, P. Zhou, Y. Chao, C. Ma, X. Bo, J. Liu and Y. Hei, *ACS Sustainable Chem. Eng.*, 2020, **8**, 13813–13822.
81 S. Wang, P. Zhou, L. Zhou, F. Lv, Y. Sun, Q. Zhang, L. Gu, H. Yang and S. Guo, *Nano Lett.*, 2021, **21**, 4262–4269.
82 H. Shang, T. Wang, J. Pei, Z. Jiang, D. Zhou, Y. Wang, H. Li, J. Dong, Z. Zhuang and W. Chen, *Angew. Chem., Int. Ed.*, 2020, **59**, 22465–22469.
83 Z. Jiang, T. Wang, J. Pei, H. Shang, D. Zhou, H. Li, J. Dong, Y. Wang, R. Cao and Z. Zhuang, *Energy Environ. Sci.*, 2020, **13**, 2856–2863.
84 X. Zu, X. Li, W. Liu, Y. Sun, J. Xu, T. Yao, W. Yan, S. Gao, C. Wang, S. Wei and Y. Xie, *Adv. Mater.*, 2019, **31**, e1808135.
85 G. Wang, J. Chen, Y. Ding, P. Cai, L. Yi, Y. Li, C. Tu, Y. Hou, Z. Wen and L. Dai, *Chem. Soc. Rev.*, 2021, **50**, 4993–5061.
86 N. Daelman, M. Capdevila-Cortada and N. López, *Nat. Mater.*, 2019, **18**, 1215–1221.
87 H. Zhang, W. Cheng, D. Luan and X. W. Lou, *Angew. Chem., Int. Ed.*, 2021, **60**, 13177–13196.
88 Y. N. Gong, L. Jiao, Y. Qian, C. Y. Pan, L. Zheng, X. Cai, B. Liu, S. H. Yu and H. L. Jiang, *Angew. Chem., Int. Ed.*, 2020, **59**, 2705–2709.
89 Z. Fu, Q. Li, X. Bai, Y. Huang, L. Shi and J. Wang, *Nanoscale*, 2021, **13**, 12233–12241.
90 H. Zhang, J. Li, S. Xi, Y. Du, X. Hai, J. Wang, H. Xu, G. Wu, J. Zhang and J. Lu, *Angew. Chem.*, 2019, **131**, 15013–15018.
91 X. Yang, J. Cheng, X. Yang, Y. Xu, W. Sun, N. Liu and J. Liu, *ACS Sustainable Chem. Eng.*, 2021, **9**, 6438–6445.
92 Y. Zhang, L. Jiao, W. Yang, C. Xie and H. L. Jiang, *Angew. Chem., Int. Ed.*, 2021, **60**, 7607–7611.
93 X. Rong, H. J. Wang, X. L. Lu, R. Si and T. B. Lu, *Angew. Chem., Int. Ed.*, 2020, **59**, 1961–1965.
94 X. Zhao, S. Huang, Z. Chen, C. Lu, S. Han, C. Ke, J. Zhu, J. Zhang, D. Tranca and X. Zhuang, *Carbon*, 2021, **178**, 488–496.
95 C. Yan, H. Li, Y. Ye, H. Wu, F. Cai, R. Si, J. Xiao, S. Miao, S. Xie and F. Yang, *Energy Environ. Sci.*, 2018, **11**, 1204–1210.
96 K. Jiang, S. Siahrostami, T. Zheng, Y. Hu, S. Hwang, E. Stavitski, Y. Peng, J. Dynes, M. Gangisetty and D. Su, *Energy Environ. Sci.*, 2018, **11**, 893–903.
97 R. Daiyan, X. Zhu, Z. Tong, L. Gong, A. Razmjou, R.-S. Liu, Z. Xia, X. Lu, L. Dai and R. Amal, *Nano Energy*, 2020, **78**, 105213.
98 Y. Cai, J. Fu, Y. Zhou, Y. C. Chang, Q. Min, J. J. Zhu, Y. Lin and W. Zhu, *Nat. Commun.*, 2021, **12**, 586.
99 W. Zheng, J. Yang, H. Chen, Y. Hou, Q. Wang, M. Gu, F. He, Y. Xia, Z. Xia, Z. Li, B. Yang, L. Lei, C. Yuan, Q. He, M. Qiu and X. Feng, *Adv. Funct.Mater.*, 2019, **30**, 1907658.
100 W. Ni, Y. Gao, Y. Lin, C. Ma, X. Guo, S. Wang and S. Zhang, *ACS Catal.*, 2021, **11**, 5212–5221.
101 Z. Wang, C. Wang, Y. Hu, S. Yang, J. Yang, W. Chen, H. Zhou, F. Zhou, L. Wang and J. Du, *Nano Res.*, 2021, 1–7.
102 X. Wang, Y. Wang, X. Sang, W. Zheng, S. Zhang, L. Shuai, B. Yang, Z. Li, J. Chen and L. Lei, *Angew. Chem., Int. Ed.*, 2021, **60**, 4192–4198.
103 B. Zhang, J. Zhang, J. Shi, D. Tan, L. Liu, F. Zhang, C. Lu, Z. Su, X. Tan and X. Cheng, *Nat. Commun.*, 2019, **10**, 1–8.

 This journal is © The Royal Society of Chemistry 2022

Published on 06 detsember 2021. Downloaded on 15.07.2024 7:26:52.

104 S.-G. Han, D.-D. Ma, S.-H. Zhou, K. Zhang, W.-B. Wei, Y. Du, X.-T. Wu, Q. Xu, R. Zou and Q.-L. Zhu, *Appl. Catal., B*, 2021, **283**, 119591.
105 J. Pei, T. Wang, R. Sui, X. Zhang, D. Zhou, F. Qin, X. Zhao, Q. Liu, W. Yan and J. Dong, *Energy Environ. Sci.*, 2021, **14**, 3019–3028.
106 Y. Ouyang, L. Shi, X. Bai, Q. Li and J. Wang, *Chem. Sci.*, 2020, **11**, 1807–1813.
107 W. Zhu, L. Zhang, S. Liu, A. Li, X. Yuan, C. Hu, G. Zhang, W. Deng, K. Zang and J. Luo, *Angew. Chem., Int. Ed.*, 2020, **59**, 12664–12668.
108 W. Ren, X. Tan, W. Yang, C. Jia, S. Xu, K. Wang, S. C. Smith and C. Zhao, *Angew. Chem., Int. Ed.*, 2019, **58**, 6972–6976.
109 J. Pei, T. Wang, R. Sui, X. Zhang, D. Zhou, F. Qin, X. Zhao, Q. Liu, W. Yan, J. Dong, L. Zheng, A. Li, J. Mao, W. Zhu, W. Chen and Z. Zhuang, *Energy Environ. Sci.*, 2021, **14**, 3019–3028.
110 W. Ni, Z. Liu, Y. Zhang, C. Ma, H. Deng, S. Zhang and S. Wang, *Adv. Mater.*, 2021, **33**, e2003238.
111 C. Lu, J. Yang, S. Wei, S. Bi, Y. Xia, M. Chen, Y. Hou, M. Qiu, C. Yuan, Y. Su, F. Zhang, H. Liang and X. Zhuang, *Adv. Funct. Mater.*, 2019, **29**, 1806884.
112 A. S. Varela, W. Ju, A. Bagger, P. Franco, J. Rossmeisl and P. Strasser, *ACS Catal.*, 2019, **9**, 7270–7284.
113 X. Zhao and Y. Liu, *J. Am. Chem. Soc.*, 2020, **142**, 5773–5777.
114 D. Karapinar, N. T. Huan, N. Ranjbar Sahraie, J. Li, D. Wakerley, N. Touati, S. Zanna, D. Taverna, L. H. Galvão Tizei and A. Zitolo, *Angew. Chem., Int. Ed.*, 2019, **58**, 15098–15103.
115 H. Xu, D. Rebollar, H. He, L. Chong, Y. Liu, C. Liu, C.-J. Sun, T. Li, J. V. Muntean, R. E. Winans, D.-J. Liu and T. Xu, *Nat. Energy*, 2020, **5**, 623–632.
116 H. Xu, D. Rebollar, H. He, L. Chong, Y. Liu, C. Liu, C.-J. Sun, T. Li, J. V. Muntean and R. E. Winans, *Nat. Energy*, 2020, **5**, 623–632.
117 D. Gao, T. Liu, G. Wang and X. Bao, *ACS Energy Lett.*, 2021, **6**, 713–727.
118 C. Lu, J. Yang, S. Wei, S. Bi, Y. Xia, M. Chen, Y. Hou, M. Qiu, C. Yuan and Y. Su, *Adv. Funct. Mater.*, 2019, **29**, 1806884.
119 Y.-G. Wang, D. Mei, V.-A. Glezakou, J. Li and R. Rousseau, *Nat. Commun.*, 2015, **6**, 1–8.
120 M. Moliner, J. E. Gabay, C. E. Kliewer, R. T. Carr, J. Guzman, G. L. Casty, P. Serna and A. Corma, *J. Am. Chem. Soc.*, 2016, **138**, 15743–15750.
121 L. Sun, V. Reddu, A. C. Fisher and X. Wang, *Energy Environ. Sci.*, 2020, **13**, 374–403.
122 S. Ren, D. Joulié, D. Salvatore, K. Torbensen, M. Wang, M. Robert and C. P. Berlinguette, *Science*, 2019, **365**, 367–369.
123 Z. Weng, J. Jiang, Y. Wu, Z. Wu, X. Guo, K. L. Materna, W. Liu, V. S. Batista, G. W. Brudvig and H. Wang, *J. Am. Chem. Soc.*, 2016, **138**, 8076–8079.
124 C. L. Yao, J. C. Li, W. Gao and Q. Jiang, *Chem.–Eur. J.*, 2018, **24**, 11051–11058.
125 S. Lin, C. S. Diercks, Y.-B. Zhang, N. Kornienko, E. M. Nichols, Y. Zhao, A. R. Paris, D. Kim, P. Yang and O. M. Yaghi, *Science*, 2015, **349**, 1208–1213.
126 Z. Weng, J. Jiang, Y. Wu, Z. Wu, X. Guo, K. L. Materna, W. Liu, V. S. Batista, G. W. Brudvig and H. Wang, *J. Am. Chem. Soc.*, 2016, **138**, 8076–8079.
127 J. Gu, C.-S. Hsu, L. Bai, H. M. Chen and X. Hu, *Science*, 2019, **364**, 1091–1094.
128 C. Costentin, M. Robert, J.-M. Savéant and A. Tatin, *Proc. Natl. Acad. Sci. U. S. A.*, 2015, **112**, 6882–6886.
129 P. Lu, Y. Yang, J. Yao, M. Wang, S. Dipazir, M. Yuan, J. Zhang, X. Wang, Z. Xie and G. Zhang, *Appl. Catal., B*, 2019, **241**, 113–119.
130 Z. Zhang, J. Xiao, X. J. Chen, S. Yu, L. Yu, R. Si, Y. Wang, S. Wang, X. Meng and Y. Wang, *Angew. Chem., Int. Ed.*, 2018, **57**, 16339–16342.
131 J. Han, P. An, S. Liu, X. Zhang, D. Wang, Y. Yuan, J. Guo, X. Qiu, K. Hou and L. Shi, *Angew. Chem.*, 2019, **131**, 12841–12846.
132 J. Wang, X. Huang, S. Xi, H. Xu and X. Wang, *Angew. Chem., Int. Ed.*, 2020, **59**, 19162–19167.
133 H. Kim, D. Shin, W. Yang, D. H. Won, H.-S. Oh, M. W. Chung, D. Jeong, S. H. Kim, K. H. Chae and J. Y. Ryu, *J. Am. Chem. Soc.*, 2021, **143**, 925–933.
134 E. A. Mohamed, Z. N. Zahran and Y. Naruta, *Chem. Commun.*, 2015, **51**, 16900–16903.
135 C. G. Margarit, C. Schnedermann, N. G. Asimow and D. G. Nocera, *Organometallics*, 2018, **38**, 1219–1223.
136 E. M. Nichols, J. S. Derrick, S. K. Nistanaki, P. T. Smith and C. J. Chang, *Chem. Sci.*, 2018, **9**, 2952–2960.
137 M. H. Ronne, D. Cho, M. R. Madsen, J. B. Jakobsen, S. Eom, E. Escoude, H. C. D. Hammershoj, D. U. Nielsen, S. U. Pedersen, M. H. Baik, T. Skrydstrup and K. Daasbjerg, *J. Am. Chem. Soc.*, 2020, **142**, 4265–4275.
138 S. Bang, Y. M. Lee, S. Hong, K. B. Cho, Y. Nishida, M. S. Seo, R. Sarangi, S. Fukuzumi and W. Nam, *Nat. Chem.*, 2014, **6**, 934–940.
139 X. Zhang, Z. Wu, X. Zhang, L. Li, Y. Li, H. Xu, X. Li, X. Yu, Z. Zhang and Y. Liang, *Nat. Commun.*, 2017, **8**, 1–8.
140 N. Morlanes, K. Takanabe and V. Rodionov, *ACS Catal.*, 2016, **6**, 3092–3095.
141 J. Choi, P. Wagner, R. Jalili, J. Kim, D. R. MacFarlane, G. G. Wallace and D. L. Officer, *Adv. Energy Mater.*, 2018, **8**, 1801280.
142 M. Zhu, J. Chen, L. Huang, R. Ye, J. Xu and Y. F. Han, *Angew. Chem., Int. Ed. Engl.*, 2019, **58**, 6595–6599.
143 M. Zhu, J. Chen, R. Guo, J. Xu, X. Fang and Y.-F. Han, *Appl. Catal., B*, 2019, **251**, 112–118.
144 Y. R. Wang, Q. Huang, C. T. He, Y. Chen, J. Liu, F. C. Shen and Y. Q. Lan, *Nat. Commun.*, 2018, **9**, 4466.
145 Y. Wu, Z. Jiang, X. Lu, Y. Liang and H. Wang, *Nature*, 2019, **575**, 639–642.
146 X. Zhang, Z. Wu, X. Zhang, L. Li, Y. Li, H. Xu, X. Li, X. Yu, Z. Zhang, Y. Liang and H. Wang, *Nat. Commun.*, 2017, **8**, 14675.
147 M. Zhu, R. Ye, K. Jin, N. Lazouski and K. Manthiram, *ACS Energy Lett.*, 2018, **3**, 1381–1386.
148 H. Wu, M. Zeng, X. Zhu, C. Tian, B. Mei, Y. Song, X.-L. Du, Z. Jiang, L. He, C. Xia and S. Dai, *ChemElectroChem*, 2018, **5**, 2717–2721.

Published on 06 detsember 2021. Downloaded on 15.07.2024 7:26:52.

149 N. Han, Y. Wang, L. Ma, J. Wen, J. Li, H. Zheng, K. Nie, X. Wang, F. Zhao, Y. Li, J. Fan, J. Zhong, T. Wu, D. J. Miller, J. Lu, S.-T. Lee and Y. Li, *Chem*, 2017, **3**, 652–664.
150 J. Wu, M. Liu, P. P. Sharma, R. M. Yadav, L. Ma, Y. Yang, X. Zou, X.-D. Zhou, R. Vajtai and B. I. Yakobson, *Nano Lett.*, 2016, **16**, 466–470.
151 J. Wu, R. M. Yadav, M. Liu, P. P. Sharma, C. S. Tiwary, L. Ma, X. Zou, X.-D. Zhou, B. I. Yakobson and J. Lou, *ACS Nano*, 2015, **9**, 5364–5371.
152 W. Wang, L. Shang, G. Chang, C. Yan, R. Shi, Y. Zhao, G. I. N. Waterhouse, D. Yang and T. Zhang, *Adv. Mater.*, 2019, **31**, e1808276.
153 Q. Wu, J. Gao, J. Feng, Q. Liu, Y. Zhou, S. Zhang, M. Nie, Y. Liu, J. Zhao, F. Liu, J. Zhong and Z. Kang, *J. Mater. Chem. A*, 2020, **8**, 1205–1211.
154 A. Majumdar and S. Sarkar, *Coord. Chem. Rev.*, 2011, **255**, 1039–1054.
155 F. Pan and Y. Yang, *Energy Environ. Sci.*, 2020, **13**, 2275–2309.
156 K. Jiang, Y. Huang, G. Zeng, F. M. Toma, W. A. Goddard III and A. T. Bell, *ACS Energy Lett.*, 2020, **5**, 1206–1214.
157 F. Li and Q. Tang, *J. Mater.Chem. A*, 2021, **9**, 8761–8771.
158 X. Guan, W. Gao and Q. Jiang, *J. Mater. Chem. A*, 2021, **9**, 4770–4780.
159 J.-B. Le, Q.-Y. Fan, J.-Q. Li and J. Cheng, *Sci. Adv.*, 2020, **6**, eabb1219.
160 H. Nymeyer and A. E. Garcia, *Proc. Natl. Acad. Sci. U. S. A.*, 2003, **100**, 13934–13939.
161 P. Ferrara, J. Apostolakis and A. Caflisch, *Proteins: Struct., Funct., Bioinf.*, 2002, **46**, 24–33.
162 J. A. Gauthier, S. Ringe, C. F. Dickens, A. J. Garza, A. T. Bell, M. Head-Gordon, J. K. Nørskov and K. Chan, *ACS Catal.*, 2018, **9**, 920–931.
163 Q. Li, Y. Ouyang, S. Lu, X. Bai, Y. Zhang, L. Shi, C. Ling and J. Wang, *Chem. Commun.*, 2020, **56**, 9937–9949.
164 S. Vijay, J. A. Gauthier, H. H. Heenen, V. J. Bukas, H. H. Kristoffersen and K. Chan, *ACS Catal.*, 2020, **10**, 7826–7835.

 This journal is © The Royal Society of Chemistry 2022